# Defining new mechanistic roles for αII spectrin in cardiac function

Received for publication, January 30, 2019, and in revised form, April 22, 2019 Published, Papers in Press, May 7, 2019, DOI 10.1074/jbc.RA119.007714

Ellen R. Lubbers[‡§¶], Nathaniel P. Murphy[‡§¶], Hassan Musa[‡], Claire Yu-Mei Huang[‖], Rohan Gupta[‡], Morgan V. Price[‡], Mei Han[‡], Georges Daoud[‡], Daniel Gratz[‡**], Mona El Refaey[‡], Xianyao Xu[‡], Nicole K. Hoeflinger[‡], Emma L. Friel[‡], Peter Lancione[‡], Michael J. Wallace[‡], Omer Cavus[‡], Samantha L. Simmons[‡], Jordan L. Williams[‡], Michel Skaf[‡], Sara N. Koenig[‡], Paul M. L. Janssen[‡¶‡‡], Matthew N. Rasband[‖], Thomas J. Hund[‡**‡‡], and Peter J. Mohler[‡¶‡‡1]

*From the [‡]Dorothy M. Davis Heart and Lung Research Institute and Frick Center for Heart Failure and Arrhythmia, [§]Medical Scientist Training Program, the Departments of [¶]Physiology and Cell Biology and [‡‡]Internal Medicine, Division of Cardiovascular Medicine, The Ohio State University College of Medicine and Wexner Medical Center, Columbus, Ohio 432310, the [‖]Department of Neuroscience and Integrative Molecular and Biomedical Sciences Graduate Program, Baylor College of Medicine, Houston, Texas 77030, and the **Department of Biomedical Engineering, The Ohio State University, Columbus, Ohio 432310*

Edited by Eric R. Fearon

**Spectrins are cytoskeletal proteins essential for membrane biogenesis and regulation and serve critical roles in protein targeting and cellular signaling. αII spectrin (*SPTAN1*) is one of two α spectrin genes and αII spectrin dysfunction is linked to alterations in axon initial segment formation, cortical lamination, and neuronal excitability. Furthermore, human αII spectrin loss-of-function variants cause neurological disease. As global αII spectrin knockout mice are embryonic lethal, the *in vivo* roles of αII spectrin in adult heart are unknown and untested. Here, based on pronounced alterations in αII spectrin regulation in human heart failure we tested the *in vivo* roles of αII spectrin in the vertebrate heart. We created a mouse model of cardiomyocyte-selective αII spectrin-deficiency (cKO) and used this model to define the roles of αII spectrin in cardiac function. αII spectrin cKO mice displayed significant structural, cellular, and electrical phenotypes that resulted in accelerated structural remodeling, fibrosis, arrhythmia, and mortality in response to stress. At the molecular level, we demonstrate that αII spectrin plays a nodal role for global cardiac spectrin regulation, as αII spectrin cKO hearts exhibited remodeling of αI spectrin and altered β-spectrin expression and localization. At the cellular level, αII spectrin deficiency resulted in altered expression, targeting, and regulation of cardiac ion channels $Na_V1.5$ and $K_V4.3$. In summary, our findings define critical and unexpected roles for the multifunctional αII spectrin protein in the heart. Furthermore, our work provides a new *in vivo* animal model to study the roles of αII spectrin in the cardiomyocyte.**

This work was supported by National Institutes of Health Grants HL135754, HL134824, HL139348, HL135096, and HL114383 (to P. J. M.), HL135096, HL134824, and HL114893 (to T. J. H.), HL137331 (to E. R. L.), and HL137325 (to N. P. M.), an Ohio State University Graduate School University Fellowship, Medical Scientist Training Program, and the Ohio State JB Project. The authors declare that they have no conflicts of interest with the contents of this article. The content is solely the responsibility of the authors and does not necessarily represent the official views of the National Institutes of Health.

This article contains Figs. S1–S16 and Table S1 and S2.

[1] To whom correspondence should be addressed: 110G DHLRI, 473 West 12th Ave., Columbus, OH 43210. Tel.: 614-292-5019; Fax: 614-247-7799; E-mail: Peter.Mohler@osumc.edu.

Cardiovascular disease is the number one cause of mortality in the United States, accounting for ~31% of all deaths (1). Although significant initiatives in both prevention and therapeutics have reduced cardiovascular mortality, the field lacks effective solutions for a host of cardiovascular phenotypes. Furthermore, the literature is just beginning to address the striking complexity of organ, cell, and molecular pathways linked with human cardiovascular disorders. Thus, there remains a clear need to understand the fundamental cellular and molecular pathways associated with normal cardiac function as well as dysfunction of critical pathways in cardiovascular disease.

Cardiac function requires finely tuned integration of myocyte mechanical and electrical pathways. Membrane-associated ion channels, transporters, receptors, signaling proteins, and cell adhesion molecules are important for cardiac function. The organization of these proteins within the vertebrate myocyte is essential for normal excitation-contraction coupling. In fact, decades of research have illustrated the role of the submembrane cytoskeleton and cytoskeletal-associated proteins in excitable cell biology (2–7). Moreover, in the heart alone, defects in myocyte cytoskeletal proteins have been linked with a host of structural and electrical phenotypes in human cardiovascular disease as well as in animal disease models (4).

Spectrins are cytoskeletal proteins, initially identified through their roles in erythrocyte structure and flexibility (8–10). In diverse tissues, spectrins act as an essential link between the actin-based cytoskeleton and membrane, serving to maintain cellular structure and polarity while providing flexibility and strength. In excitable cells and nonexcitable cells, spectrins form complexes with ankyrins and membrane-associated proteins, playing essential roles in the localization and regulation of critical ion channels and transporters (11–14). In humans, there are five β but only two α spectrin genes (15). *SPTAN1* encodes nonerythrocytic αII spectrin, which forms functional heterotetramers with β spectrins (16). αII spectrin has been extensively studied in neurons due in part to its link to human neurologic disease. Variants in *SPTAN1* are linked to

early infantile epileptic encephalopathy, type 5 (EIEE5)[2] or West Syndrome, characterized by refractory seizures, intellectual arrest/regression, agenesis of the corpus callosum, and hypomyelination, carrying a poor prognosis (11, 17, 18). Beyond the brain, recent work has defined roles for β-spectrins in cardiac structure, excitability, and signaling and linked dysfunction in β spectrin pathways with both acquired and congenital forms of human cardiovascular disease (19, 20). In contrast, the number of studies on αII spectrin in heart are limited (21–26), and the *in vivo* roles of cardiac α spectrins are essentially unstudied.

Here, we report dysregulation of αII spectrin in human heart failure. Moreover, using a newly engineered model of cardiomyocyte-specific deletion of αII spectrin, we illustrate the role of αII spectrin in normal cardiac physiology. αII spectrin cKO mice display both structural and electrical phenotypes at baseline that are intensified by physiological and pathological stress. Furthermore, we illustrate striking post-transcriptional roles for αII spectrin for global spectrin family protein regulation and unanticipated roles for αII spectrin in ion channel expression, targeting, and regulation. Together, our findings define critical *in vivo* roles for αII spectrin in the stabilization of the cardiomyocyte spectrin network, ion channel regulation, cardiac electrophysiology, structure, function, and stress response.

## Results

### αII spectrin is dysregulated in human heart failure

To evaluate potential dysregulation of αII spectrin in human cardiovascular disease, we performed immunoblot experiments on failing and nonfailing human left ventricle. Spectrins are cleaved by both calpain and caspase, forming specific degradation products (27). Specifically, αII spectrin is proteolytically cleaved by both caspase and calcium-activated calpain, forming ~120- and ~150-kDa degradation products, respectively (27, 28). Notably, the ~150-kDa (calpain-mediated) cleavage product of αII spectrin was significantly increased in both ischemic and nonischemic heart failure (HF) samples compared with samples from nonfailing hearts (Fig. 1, *A–D*). Furthermore, levels of the ~120-kDa (caspase-mediated) cleavage were increased in human HF samples compared with samples from nonfailing hearts ($p < 0.05$, $n = 3$ nonfailing, 6 HF). Levels of full-length αII spectrin were similar between samples likely due to the observed trend toward a significant transcriptional up-regulation of αII spectrin in disease (Fig. S1). In summary, cardiac αII spectrin degradation products are significantly increased in human heart failure.

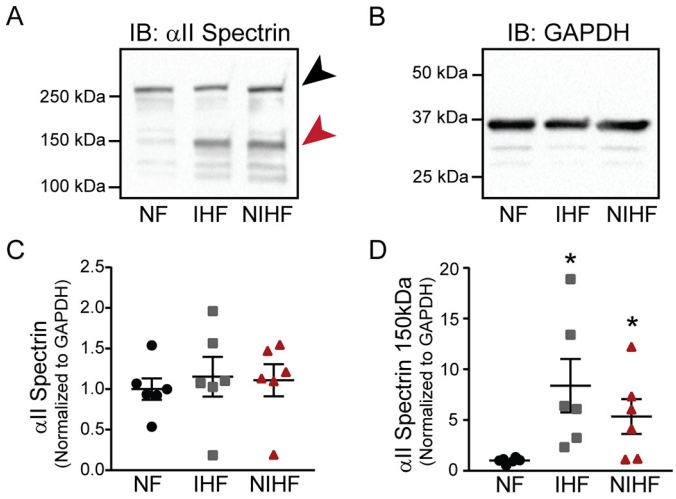


**Figure 1. Altered αII spectrin regulation in human heart failure.** *A* and *B*, representative, and *C* and *D*, quantification of immunoblots of human control (nonfailing) and ischemic (*IHF*) or nonischemic (*NIHF*) failing left ventricular tissue for αII spectrin, normalized to GAPDH. *C*, levels of full-length αII spectrin (*black arrowhead*), are unchanged, whereas for *D*, levels of the 150-kDa degradation product (*red arrowhead*) are increased in ischemic and nonischemic failing human LV ($n = 6, 6, 6$ for NF, IHF, NIHF LV, respectively, $p$ value $<0.0001$ for the 150-kDa degradation product). Values are represented as mean ± S.E.

### Creation and validation of in vivo model of cardiomyocyte αII spectrin deficiency

Based on the critical role of spectrins in excitable cells and dysregulation in heart failure (Fig. 1), we investigated the role of αII spectrin for *in vivo* cardiac function. To date, due to the embryonic lethality of global αII spectrin knockout mice (29), the role of αII spectrin in the adult heart is unknown and unstudied. Thus, we generated a cardiomyocyte-specific αII spectrin mouse knockout model (αII spectrin cKO) using the Cre-lox system in which exon 8 of *Sptan1* is flanked by LoxP sites (30) and the expression of Cre recombinase is driven under the α-myosin heavy chain promoter (Fig. 2*A*) (31).

αII spectrin cKO mice are viable, showed no gross visible phenotypes, and reproduced normally. As expected, cardiomyocyte preparations from αII spectrin cKO mouse myocytes displayed near-complete loss of αII spectrin protein expression (Fig. 2, *B–D*). This loss was selective for cardiomyocytes as αII spectrin protein levels were similar between control and αII spectrin cKO cerebellum (Fig. 2, *E–G*) and skeletal muscle. In the control mouse heart, αII spectrin is highly expressed and localizes to the Z-disc, lateral membrane, and intercalated disc (Fig. 2, *H* and *I*). Notably, this intracellular distribution does not completely overlap with αI spectrin (localized to the Z-disc and lateral membrane, absent from the intercalated disc (25)) suggesting potential unique roles for αII spectrin *versus* αI spectrin. Consistent with immunoblot data, αII spectrin cKO mice displayed complete loss of αII spectrin in the cardiomyocyte by immunofluorescence (Fig. 2*J*). Thus, the newly generated knockout mouse line provides a viable model to study *in vivo* αII spectrin deficiency in cardiomyocytes.

### αII spectrin cKO mice display cardiac dysfunction

To test the *in vivo* role of αII spectrin in vertebrate heart, we performed detailed cardiac structural and functional phenotyp-

[2] The abbreviations used are: EIEE5, early infantile epileptic encephalopathy, type 5; cKO, conditional knockout; PVC, premature ventricular contraction; APA, action potential amplitude; $dV/dT_{max}$, maximum upstroke velocity; APD, action potential duration; $I_{TO}$, transient outward potassium current; $I_{Na}$, sodium current; ECM, extracellular matrix; TAC, transverse aortic constriction; HF, heart failure; LVID, left ventricle internal diameter; LVPW, left ventricle posterior wall; QTc, corrected QT interval; TUNEL, TdT-mediated dUTP nick-end labeling; Ctl, control; GAPDH, glyceraldehyde-3-phosphate dehydrogenase.

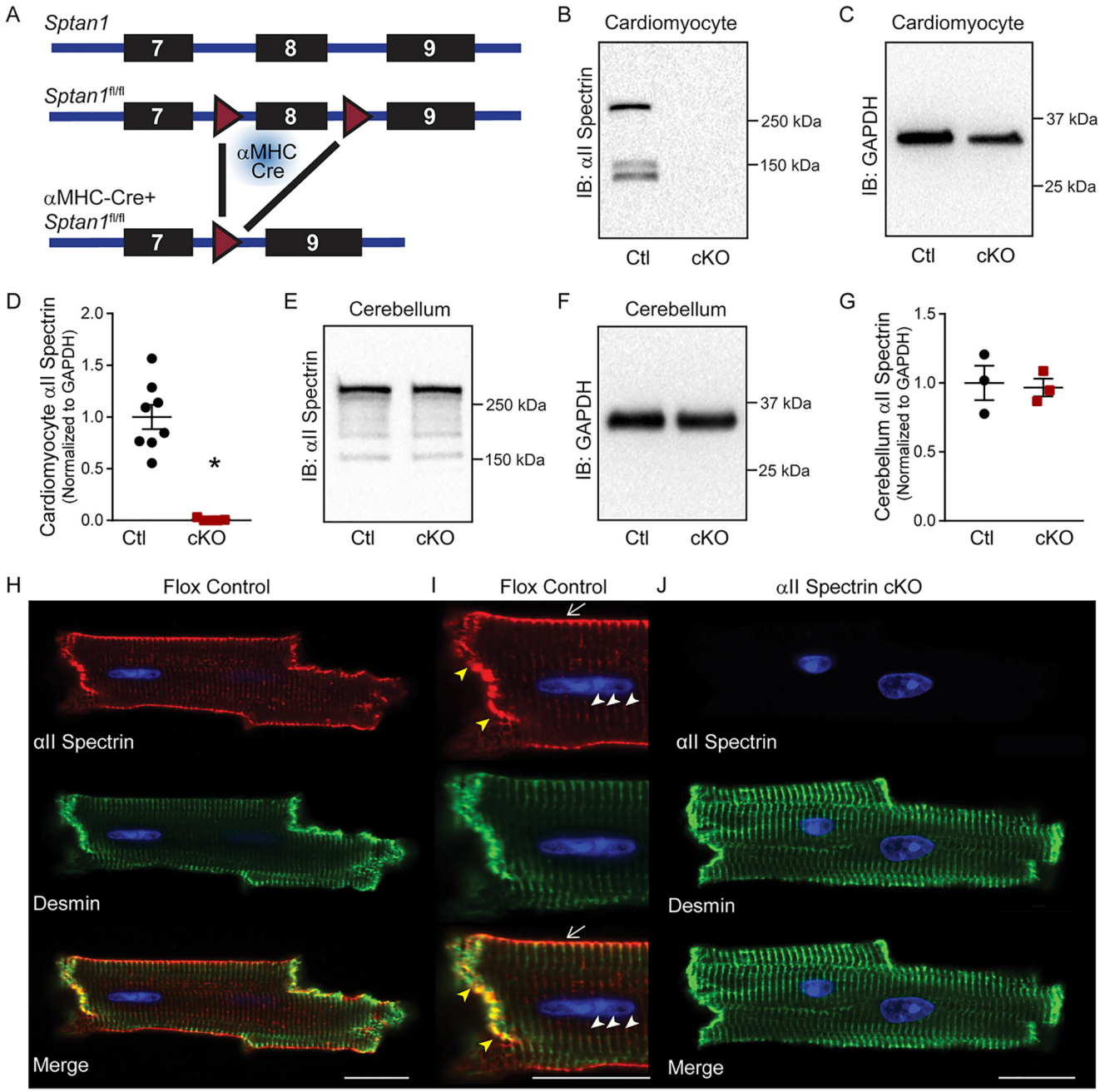


**Figure 2. Generation and validation of αII spectrin cKO mice.** *A,* strategy for cardiomyocyte-specific knockout of αII spectrin in mice. *B–G,* representative and quantification of immunoblots for αII spectrin normalized to glyceraldehyde-3-phosphate dehydrogenase (*GAPDH*) in isolated adult ventricular myocytes and cerebellum from αII spectrin cKO and control mice. Results demonstrate (*B–D*) reduction of full-length (>250 kDa) and degraded (~150 kDa) αII spectrin from isolated adult ventricular myocytes from αII spectrin cKO mice compared with control mice ($n = 8.5$ for control and αII spectrin cKO mice, respectively, $p < 0.0001$). *E–G,* no differences in αII spectrin levels were observed in cerebellum. Values are represented as mean ± S.E. *H–J,* staining of αII spectrin (*red*) and desmin (*green*) in adult cardiomyocytes isolated from (*H*) control and (*J*) αII spectrin cKO mice. *I,* magnified image of control myocytes demonstrates localization of αII spectrin at lateral membrane (*white arrows*), Z-lines (*white arrowheads*), and intercalated disc (*yellow arrowheads*). *Scale bars* = 20 μm.

ing of αII spectrin cKO mice and control littermates. In adult mice (20–24 weeks of age), we observed a significant decrease in stroke volume, ejection fraction, and fractional shortening, indicative of early stages of heart failure and/or cardiac remodeling (Fig. 3, *A–F*). Furthermore, αII spectrin cKO mice displayed cardiomyocyte hypertrophy, as assessed by histologic analysis of cross-sectional cardiomyocyte size (Fig. 3*L*, Fig. S2). However, this did not translate into gross increases in heart weight, even when normalized to body weight or to tibia length (Fig. S3). Histologically, we observed increased cardiac fibrosis in αII spectrin cKO mice, as assessed by automated quantification of Masson's Trichrome-stained heart samples (Fig. 3, *I–K*). Fibrosis was not accompanied by an increase in apoptosis, as assayed by TUNEL staining (Fig. S4). Notably, this dysfunction develops with age, as αII spectrin hearts from younger mice (12–16 weeks of age) displayed no significant changes in cardiac structure or function and no fibrosis, necrosis, or hypertrophic phenotypes (Fig. S5). Thus, αII spectrin deficiency promotes an age-dependent decline in cardiac ejection fraction and increased cardiac fibrosis.

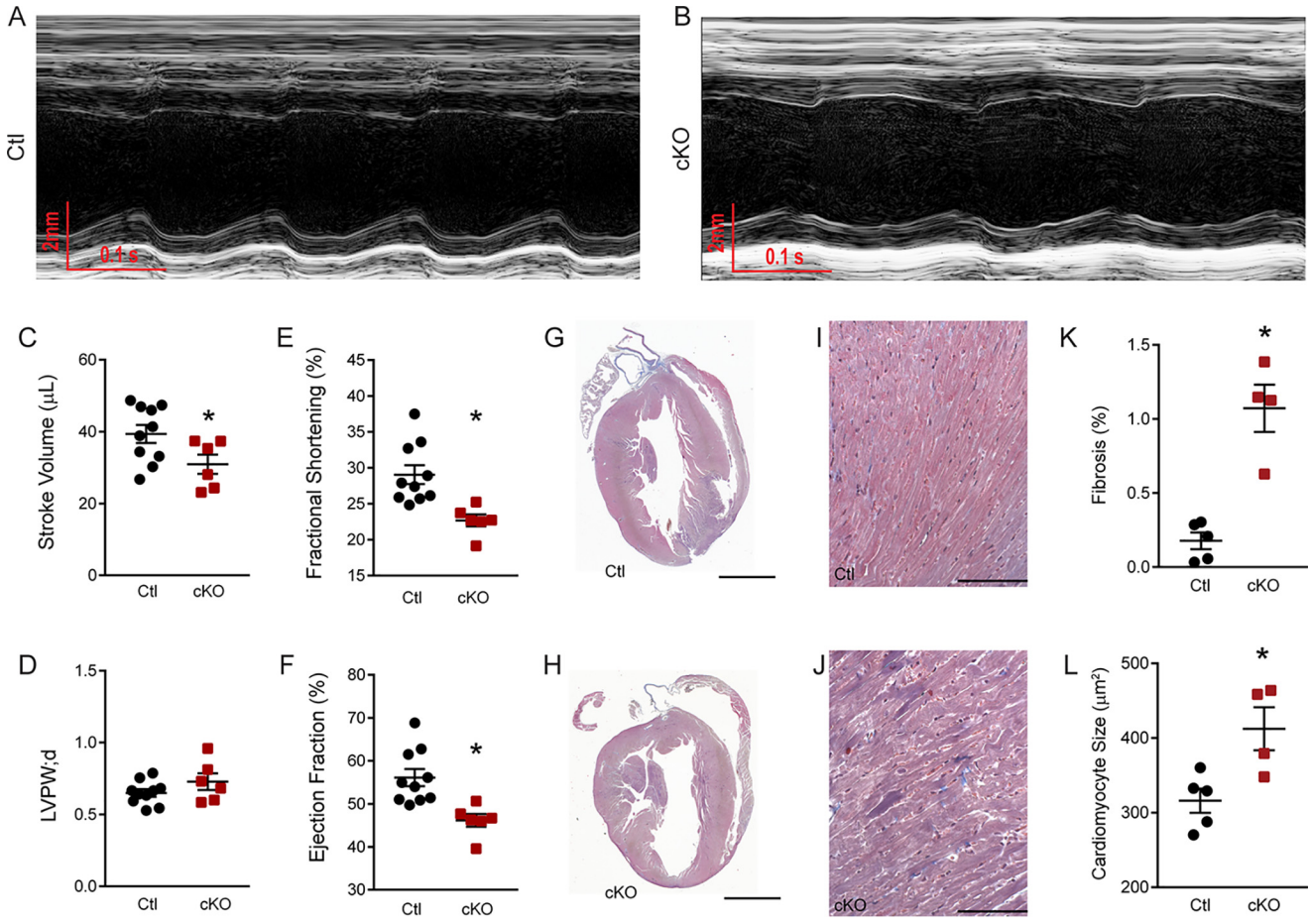


**Figure 3. αII spectrin cKO mice exhibit age-related cardiac function decline.** *A–F*, by 20 weeks of age, αII spectrin cKO mice demonstrate a significant decrease in cardiac function, as evaluated by echocardiography. *A* and *B*, M-mode traces from adult (*A*) control and (*B*) αII spectrin cKO mice. *D*, wall thickness is unchanged, whereas *C*, stroke volume; *E*, fractional shortening; and *F*, ejection fraction are decreased in αII spectrin cKO mice when compared with littermate controls ($n = 10$ and 6 for control and αII spectrin cKO mice, respectively). *G-L*, αII spectrin cKO mice exhibit cellular hypertrophy and increased fibrosis compared with littermate controls. *G* and *H*, representative images of cardiac structure in control (*G*) and αII spectrin (*H*) cKO mice. *Scale bar* = 2 mm. *I* and *J*, representative Masson's trichrome-stained cardiac tissue from control (*I*) and αII spectrin (*J*) cKO mice demonstrating increased fibrosis (*K*). *Scale bars* = 100 μm. *L*, αII spectrin cKO mice have increased average cross-sectional myocyte size ($n = 5$ and 4 for control and αII spectrin cKO mice, respectively). All values are represented as mean ± S.E. * indicates a statistical differences from controls, $p < 0.05$.

### *αII spectrin cKO mice display in vivo electrical dysfunction*

We next tested the impact of αII spectrin deficiency on cardiac excitability. We observed electrical dysfunction in αII spectrin cKO mice, regardless of age. In young 12–16–week-old mice, prior to structural dysfunction, we observed ECG phenotypes in αII spectrin cKO mice compared with control mice including minor, but significant increases in P wave and QRS duration by conscious recordings (Table S1; no change in QRS by DSI telemetry), indicating slowed conduction through the atria and ventricles. Notably, this slowed conduction is not associated with reduced levels or altered localization of connexin 43 (Fig. S6).

Treatment of conscious αII spectrin cKO, but not control animals with epinephrine revealed significant differences in heart rate as well as PR, QT, and rate corrected QT (QTc) intervals when compared with control littermates (Table S1). Furthermore, epinephrine-treated αII spectrin cKO mice (but not control littermates) displayed arrhythmia phenotypes including sustained runs of premature ventricular contractions (PVCs) (Fig. 4, *A–C*). In summary, 12–16–week-old αII spectrin cKO mice display defects in electrical activity that precede cardiac structural and functional phenotypes. Furthermore, electrical phenotypes are increased by catecholamine treatment.

### *αII spectrin is required for normal myocyte excitability*

Based on *in vivo* αII spectrin cKO mouse phenotypes, we investigated electrical properties at the individual myocyte level. Compared with control myocytes, we observed statistically significant changes in action potential duration (APD) at 50, 75, and 90% repolarization ($APD_{50}$, $APD_{75}$, and $APD_{90}$, respectively) or in maximum upstroke velocity (dV/dT) in αII spectrin cKO myocytes (Fig. S7, *A–C*; 0.5 Hz). Furthermore, we observed a statistically significant increase in action potential amplitude (APA) in αII spectrin cKO myocytes compared with control cells (Fig. S7*D*). These changes occurred in the absence of changes in resting membrane voltage (Fig. S8). Notably, we observed a failure of αII spectrin cKO myocytes to initiate an action potential at higher stimulation frequencies (Fig. S7, *E–G*). For example, unlike control myocytes that initiated normal action potentials at frequencies up to 10 Hz, αII spectrin cKO myocytes began failing to excite at just 2 Hz, indicating a

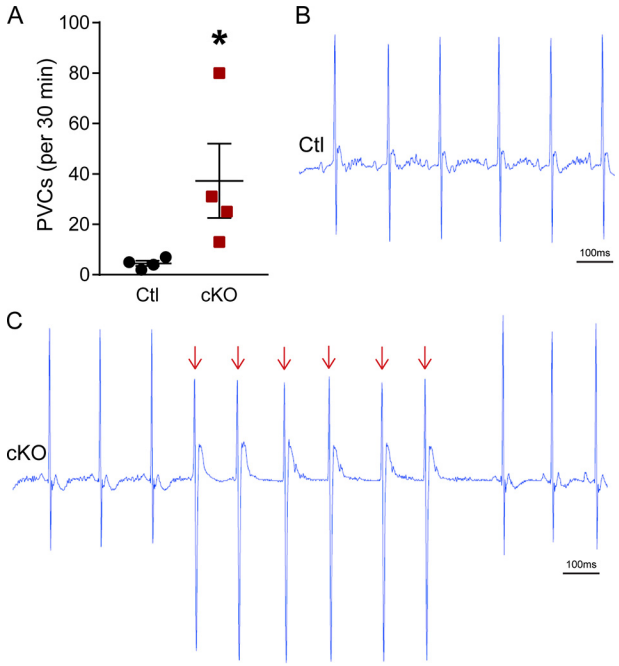


**Figure 4. Cardiac αII spectrin loss results in arrhythmia.** *A*, αII spectrin cKO mice show an increase in premature ventricular contractions (*PVCs*) following epinephrine injection compared with control littermates at 12–16 weeks of age, before structural changes. *B* and *C*, sample ECG traces from control (*B*) or αII spectrin (*C*) cKO mice. *Red arrows* indicate PVCs ($n = 4$ and 4 for αII spectrin cKO and controls, respectively). Values are represented as mean ± S.E. * indicates a significant difference from controls.

key role of αII spectrin in myocyte excitability (Fig. S7*G*). In summary, αII spectrin cKO myocytes display multiple electrical phenotypes.

### *Defining αII spectrin pathways in heart: αII spectrin is required for cardiac spectrin family regulation*

Our findings support significant *in vivo* and cellular defects in the absence of cardiac αII spectrin. We therefore directly tested the impact of αII spectrin deficiency on spectrin family regulation in heart. Consistent with our hypothesis, β spectrin proteins (obligate α spectrin-binding partners) were significantly reduced in αII spectrin cKO cardiomyocytes. We observed a 77.9% reduction in βI spectrin protein levels with βII spectrin protein levels reduced 93.2% (Fig. 5, *A–D*). Remaining βII spectrin was normally localized (Fig. 5*H*). Normal mRNA expression of βI (*Sptb*) and βII (*Sptbn1*) spectrin (Fig. 5*G*) support that altered protein levels are due to post-transcriptional regulation of β spectrins. αI spectrin, a protein unique to mammals, is structurally similar to αII spectrin, having likely arisen from a gene duplication of αII spectrin (32). Notably, in cardiomyocytes lacking αII spectrin, αI spectrin is strongly up-regulated at both transcript (Fig. 5*G*) and protein levels (Fig. 5, *E* and *F*).

In control cardiomyocytes, αI spectrin localizes to the Z-disc and lateral membrane, and is absent from the intercalated disc (Fig. 5, *I* and *J*). However, in αII spectrin cKO cardiomyocytes, αI spectrin is present at the intercalated disc (Fig. 5, *I* and *J*), supporting a putative compensatory role of αI spectrin in the αII spectrin cKO model. In summary, our data support a key role of αII spectrin expression for the normal regulation of both βI spectrin and βII spectrin expression in cardiomyocytes. Moreover, our findings support that αI spectrin levels are significantly increased in αII spectrin cKO heart as a potential compensatory mechanism to preserve cardiac function. However, our data suggest that this compensatory pathway is insufficient to restore normal function to αII spectrin cKO mice, potentially due to the inability of αI spectrin to associate with cardiac αII spectrin-binding partners.

### *αII spectrin is required for cardiac $Na_V1.5$ expression and function*

Spectrin dysfunction is linked with altered voltage-gated $Na_v$ channel regulation in the heart and brain (2, 3, 6, 33–35). We therefore tested the impact of αII spectrin-deficiency on cardiac $Na_v1.5$ regulation. $Na_v1.5$ expression was significantly reduced in αII spectrin cKO hearts compared with hearts from control littermates (Fig. 6, *A* and *B*; reduced 59.5% when normalized for total protein expression). This decrease was likely due to post-translational dysregulation, as mRNA levels of *Scn5a* (encoding $Na_V1.5$) were unchanged between control and αII spectrin hearts (Fig. 6*C*). In the control heart, $Na_v1.5$, whereas present at multiple membrane domains, is preferentially expressed at the intercalated disc membrane (Fig. 6*D*). In αII spectrin cKO hearts, we observed modestly decreased intercalated disc staining relative to lateral membrane expression of $Na_v1.5$ (Fig. 6, *D* and *E*). However, neither immunoblot nor immunofluorescent microscopy are quantitative measures of functional $Na_V1.5$. To determine the function of the remaining $Na_V1.5$, analysis by single-cell electrophysiology was conducted, which revealed nearly a 2-fold decrease in peak $I_{Na}$ in αII spectrin cKO myocytes compared with littermate controls (Fig. 7, *A* and *B*). However, we observed no difference in voltage-
dependent inactivation or time-dependent recovery from inactivation between myocytes from control and αII spectrin cKO hearts (Fig. 7, *C* and *D*). In summary, αII spectrin is required for normal $Na_v1.5$ expression, localization, and function in mouse heart.

### *Identification of putative αII spectrin-dependent cardiac pathways*

Reduced $Na_v1.5$ ($I_{Na}$) in αII spectrin cKO hearts (Figs. 6 and 7) supports the observed decrease in αII spectrin cKO myocyte excitability (Fig. S7, *E–G*), but is striking in the context of a normal $dv/dt_{max}$. As assessed by an unbiased partial least-squares regression analysis using the Hund-Rudy action potential model (36–39), $Na_v1.5$-dependent dysregulation alone is unlikely to produce observed experimental data from control and αII spectrin cKO action potential measurements (*e.g.* APD, APA, and $dv/dt_{max}$). Our computational analyses strongly predicted secondary current alterations in αII spectrin cKO myocytes, most specifically associated with several repolarizing potassium currents.

To support the computational model, we performed transcriptional analysis of mRNA expression of ion channel subunits in 12–16–week-old αII spectrin cKO *versus* control littermate hearts. In support of the modeling predictions, we observed significant changes in ion channel subunits involved

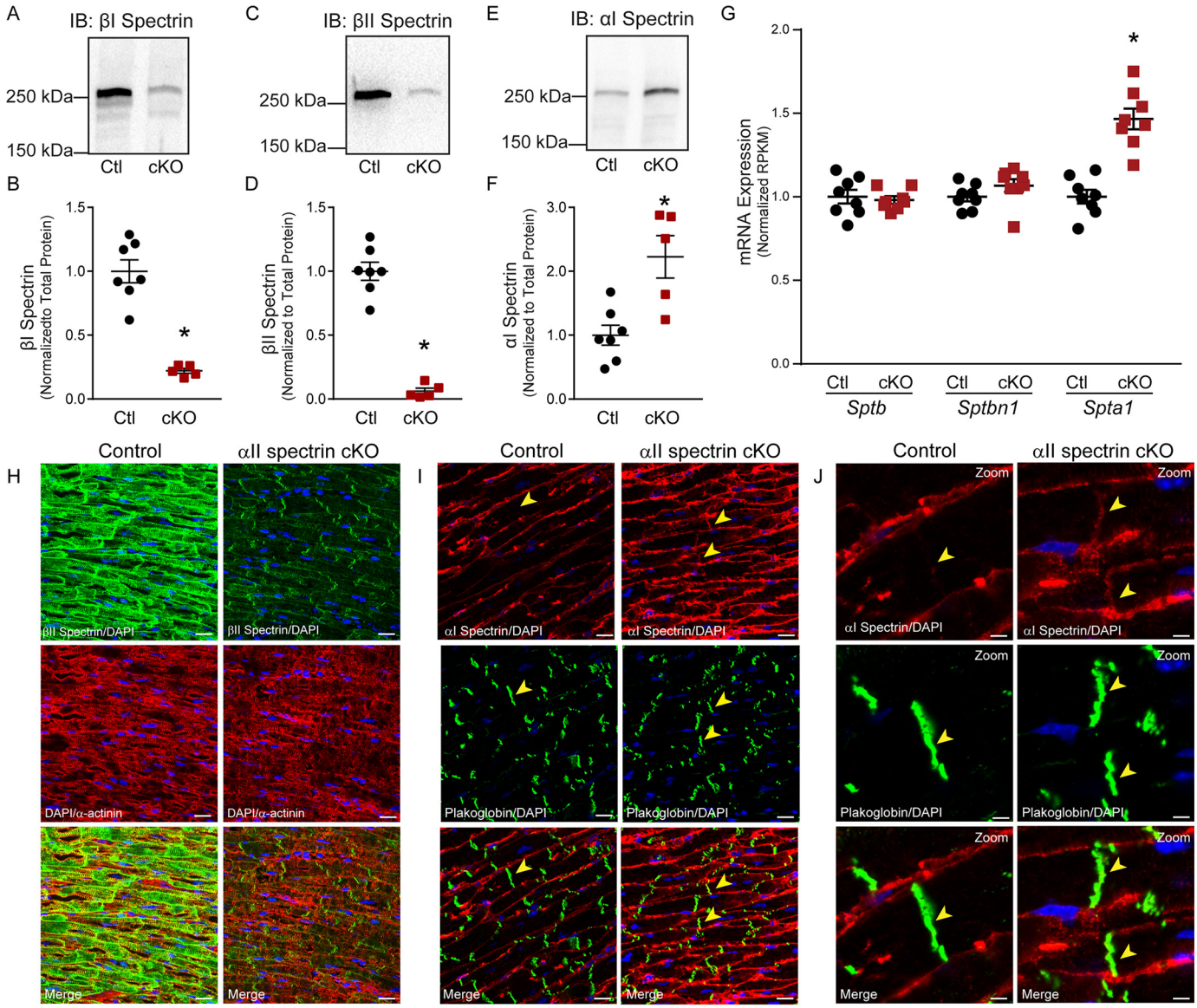


**Figure 5. Loss of cardiac αII spectrin results in broad spectrin dysregulation.** *A*, *C*, and *E*, representative, and *B*, *D*, and *F*, quantification, of immunoblots of cardiomyocytes for βI, βII, and αI spectrin ($n = 7$ and 5 for control and αII spectrin cKO, respectively, $p$ value $<0.0001$, $<0.0001$, $= 0.043$ for βI, βII, and αI spectrin, respectively). *G*, mRNA expression of *Sptb, Sptbn1,* and *Spta1* in adult cardiac tissue ($n = 8$ and 8, $p = 0.57$). *H–J*, immunofluorescence staining of βII (*H*) and αI spectrin and plakoglobin (*I* and *J*) in ventricular tissue from control and αII spectrin cKO mice demonstrating increased intercalated disc localization of αI spectrin (*yellow arrowhead*) in αII spectrin cKO tissue compared with controls. *Scale bar* = 20 μm. *J,* magnified images of intercalated discs. *Scale bar* = 5 μm.

in cardiac repolarization, particularly potassium channel α- and β-subunits (Fig. S9). Analysis of mRNA expression of *Kcnd2* (encoding $K_V4.2$) and *Kcnd3* (encoding $K_V4.3$), major contributors to $I_{K,peak,}$ $I_{TO,fast}$, revealed normal expression of *Kcnd3*, but a 0.57-fold decrease in *Kcnd2* expression in αII spectrin cKO hearts (Fig. S9). Additionally, we observed a down-regulation of $K_V1.7$ (*Kcna7*), a potassium channel subunit that modulates both $I_{Kur}$ and $I_{TO}$ in αII spectrin cKO hearts. Although we did not observe a difference in the resting membrane potential of isolated αII spectrin cKO cardiomyocytes (Fig. S8), there was a significant down-regulation of $K_{ir}2.1$ (*Kcnj2*) in αII spectrin cKO hearts compared with controls. Furthermore, we observed increased expression of the two-pore potassium channel TREK1 (*Kcnk2*), but not TASK1 (*Kcnk3*) (Fig. S9) in αII spectrin cKO hearts. Similarly, GIRK1 (*Kcnj3*) expression was decreased, whereas GIRK4 (*Kcnj5*) expression was unchanged in αII spectrin cKO hearts. *Kcne1*, linked with long QT syndrome type 5 (LQT5) showed increased expression, whereas *Kcnq1*, which is linked with long QT syndrome type 1, is unchanged in αII spectrin cKO hearts. Finally, *Kcnip2* (Kchip2), *Kcnb1* (contributing to $I_{K,SS}$), *Kcna5* (contributing to $I_{Kur}$), *Kcnj8* ($K_{ir}6.1$), *Kcnj11* ($K_{ir}6.2$), *Kcnj12* ($K_{ir}2.2$), and *Kcnj14* ($K_{ir}2.4$) were all similarly expressed between control and αII spectrin cKO hearts (Fig. S9). Thus, whereas we observed dysregulated expression of many potassium channels, many remained unchanged, demonstrating a selective disruption of potassium channel subunit expression in αII spectrin cKO hearts.

Beyond potassium channel subunits, we observed alterations in other ion channel subunits. Although the mRNA expression

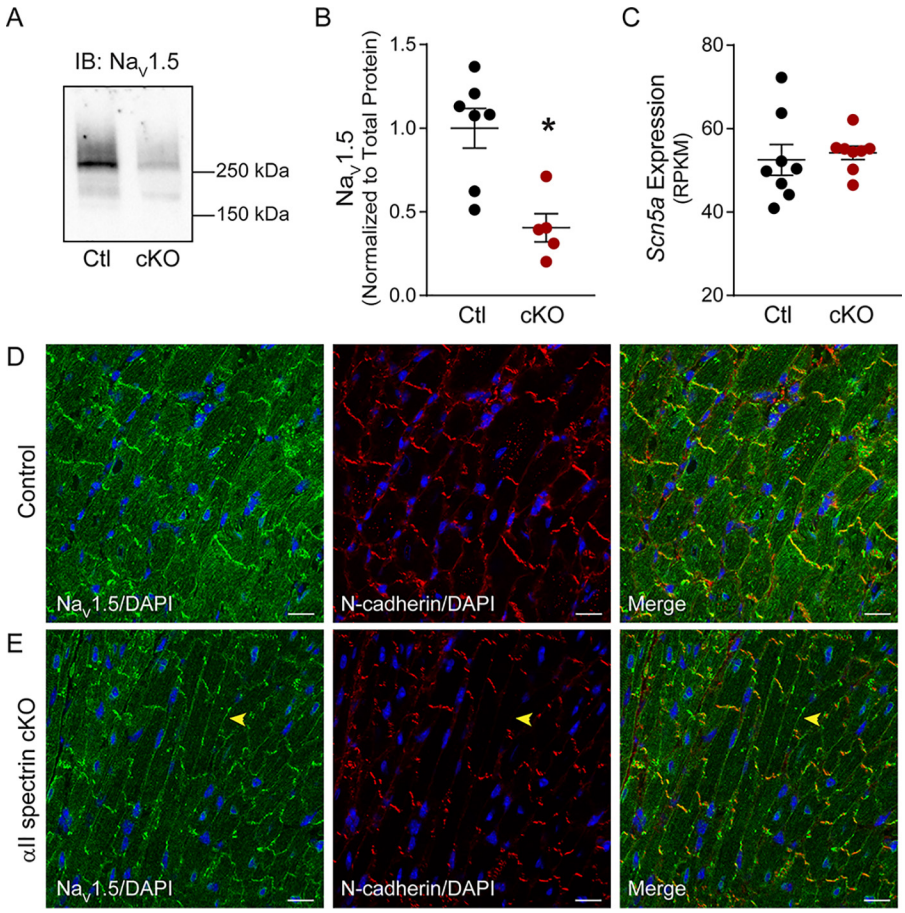


**Figure 6. Cardiac αII spectrin loss alters Na$_V$1.5 expression and localization.** *A*, representative, and *B*, quantification, of immunoblots of isolated adult ventricular myocytes for Na$_V$1.5 ($n = 7$ and 5 for control and αII spectrin cKO, respectively, $p < 0.005$). *C*, mRNA expression of *Scn5a* in adult cardiac tissue ($n = 8$ and 8; $p = 0.57$). Values are represented as mean ± S.E. *D* and *E*, staining of Na$_V$1.5 and N-cadherin in ventricular tissue from control (*D*) and αII spectrin (*E*) cKO mice showing increased lateral membrane localization (*yellow arrowhead*), compared with intercalated disc localization in αII spectrin cKO tissue. *Scale bar* = 20 μm.

of the α-subunit of Na$_V$1.5, *Scn5a*, was unchanged, the expression of the β1-subunit, *Scn1b*, was up-regulated ~2-fold in αII spectrin cKO hearts (Fig. S9). Furthermore, we noted an increase in the expression of two α subunits of the L-type calcium channel (*Cacna1s* and *Cacna1c*) accompanied by an up-regulation of the β1 (*Cacnb1*) and β3 (*Cacnb3*) subunits in αII spectrin cKO hearts (Fig. S9). In summary, consistent with computational modeling, transcriptional analysis of αII spectrin cKO hearts illustrates alterations in multiple unexpected cardiac ion channels, with a notable association with cardiac $K^+$ channels.

### αII spectrin cKO myocytes display altered repolarizing potassium currents

Based on modeling and transcript analyses, we hypothesized that select potassium currents may be altered in αII spectrin cKO hearts. In line with our data showing no difference in resting membrane voltage (Fig. S8), we observed no change in $I_{K1}$ between genotypes (Fig. 8, *A–C*). We did, however, observe significant decreases in $I_{TO}$ at both peak ($I_{TO,peak}$) and steady-state potassium currents ($I_{TO,SS}$) in αII spectrin cKO mice compared with littermate controls (Fig. 8, *D–F*). In further support of a role for αII spectrin in potassium channel regulation, we observed a significant increase in protein expression of K$_V$4.3 (Fig. 9, *A* and *B*). Of note, the increased expression of K$_V$4.3 in αII spectrin cKO mice was accompanied by more diffuse localization of K$_V$4.3 when compared with control mice (Fig. 9, *C* and *D*), suggesting a potential role for αII spectrin in K$_V$4.3 trafficking and/or localization. In summary, these data support an unexpected role for αII spectrin in regulation of cardiomyocyte potassium currents. Future experiments will be critical to define the mechanistic relationship for this regulation (direct *versus* compensatory due to $I_{Na}$ loss).

### αII spectrin associates with Na$_V$1.5 and K$_V$4.3

To investigate the relationship of αII spectrin with ion channel subunits underlying $I_{Na}$ and $I_{TO}$, we examined potential association between αII spectrin and Na$_V$1.5 and K$_V$4.3. We observed association of αII spectrin with both Na$_V$1.5 and K$_V$4.3 in co-immunoprecipitation experiments from detergent-soluble lysates of adult mouse heart (Fig. S10, *A* and *B*). In contrast, we observed no association of the structurally similar αI spectrin with Na$_V$1.5 or K$_V$4.3 in parallel co-immunoprecipitation experiments (Fig. S10, *C* and *D*). Thus, in addition to supporting association of αII spectrin with multiple ion channel subunits, these new data suggest selectivity of α spectrin polypeptides for myocyte membrane targets. Furthermore, these data suggest that αI spectrin may not completely compensate for loss of αII spectrin in the αII spectrin cKO mouse model. Future experiments will be important to define the

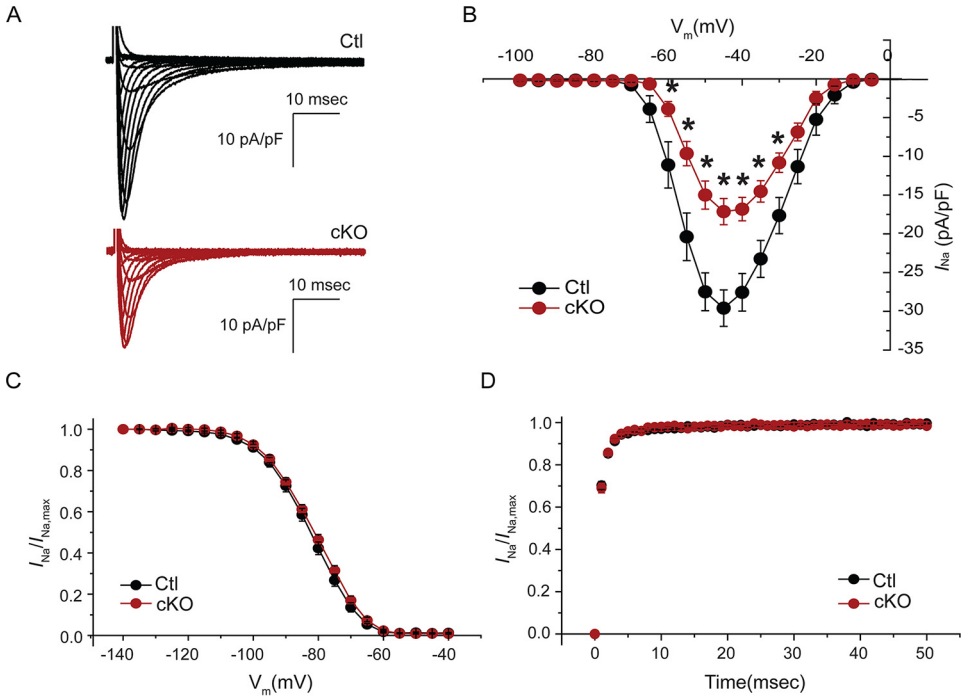


**Figure 7. Cardiac αII spectrin is essential for $I_{Na}$.** *A,* representative recordings of whole cell $I_{Na}$ from cardiomyocytes isolated from 12–16–week-old control and αII spectrin mice. *B,* current-voltage relationship of $I_{Na}$ in αII spectrin cKO and control ventricular myocytes. *C,* voltage-dependent inactivation, and *D,* time-dependent recovery, of $I_{Na}$ in αII spectrin cKO and control adult ventricular myocytes. No significant differences were observed in $V_{1/2}$ as determined by Boltzmann fits of the steady-state voltage-dependent inactivation or time-dependent recovery ($n = 3$ and 3; $n = 11$ and 11 for control and αII spectrin cKO, respectively). Values are represented as mean ± S.E. * indicates a statistical differences from controls.

mechanisms (direct *versus* indirect) and structural requirements for αII spectrin association with $Na_v1.5$ and $K_v4.3$.

### *Key cardiac regulatory pathways are altered in αII spectrin hearts*

As heart failure and arrhythmia are complex pathways involving the interplay between structural, membrane, signaling, and transcriptional pathways, we investigated αII spectrin-dependent transcriptional pathways in heart in 12–16–week-old mice, prior to cardiac electrical or structural remodeling using RNAseq (Fig. S11). Using GO Pathway analysis, we identified significantly altered regulation of many pathways, including several that may be relevant to the observed phenotypes of αII spectrin cKO mice, such as extracellular matrix organization, cell adhesion, voltage-gated channel activity, and collagen metabolic process. We focused on the dysregulation in two major transcript classes. First, several cardiac intracellular proteases including calpains and caspases, known to regulate neuronal and cardiac spectrins (24, 27, 40, 41), were significantly altered (Fig. S12*A*). Second, we observed significant alterations in transcripts associated with extracellular matrix (ECM) organization and remodeling (Fig. S12*B*). For example, we observed significant transcriptional up-regulation of TIMP1 (over 12-fold) that is essential for membrane metalloprotease regulation. Additionally, increased RNA expression of many collagens (Fig. S12*C*) is consistent with increased fibrosis and with increased ECM turnover. Thus, consistent with a critical role of αII spectrin for cardiac remodeling, αII spectrin cKO mice display significant alterations in key pathways that promote cardiac protein turnover and ECM remodeling, thus promoting heart failure phenotypes. Furthermore, established markers of cardiac hypertrophy were significantly altered, foreshadowing the increased cardiomyocyte size observed in older (20–24–week-old) mice (Fig. S13). We hypothesize that these changes serve to augment and/or accelerate phenotypes in αII spectrin cKO mice.

### *αII spectrin mice display mortality and severe cardiac phenotypes in response to stress*

αII spectrin levels are dysregulated in human HF. Moreover, αII spectrin cKO mice display significant structural and electrical phenotypes at baseline and in response to catecholaminergic stress and aging. Furthermore, in addition to observing alterations in critical global spectrin pathways in αII spectrin mice, we also observed alterations in pathways that would favor structural and electrical remodeling. We used a well-validated model for afterload-induced heart failure to test the hypothesis that αII spectrin cKO mice would display accelerated disease phenotypes in response to stress. When using our standard protocol that produces heart failure in 6–8 weeks with no early mortality (5), ~75% of αII spectrin cKO mice died within 2 weeks of transverse aortic constriction (TAC).

Based on the high mortality of αII spectrin cKO mice following standard TAC, a less severe model of pressure overload (using a 25-gauge constriction) was performed. Consistent with a critical role for αII spectrin in normal cardiac function, αII spectrin cKO mice displayed an accelerated heart failure phenotype when compared with control mice following TAC (Fig. 10). Notably, αII spectrin cKO TAC mice exhibit accelerated and decreased contractility (decreased ejection fraction, Fig. 10*A*) and cardiac dilation (increased left ventricular internal diameter (LVID) (Fig. 10*B*)), without compensatory hypertro-

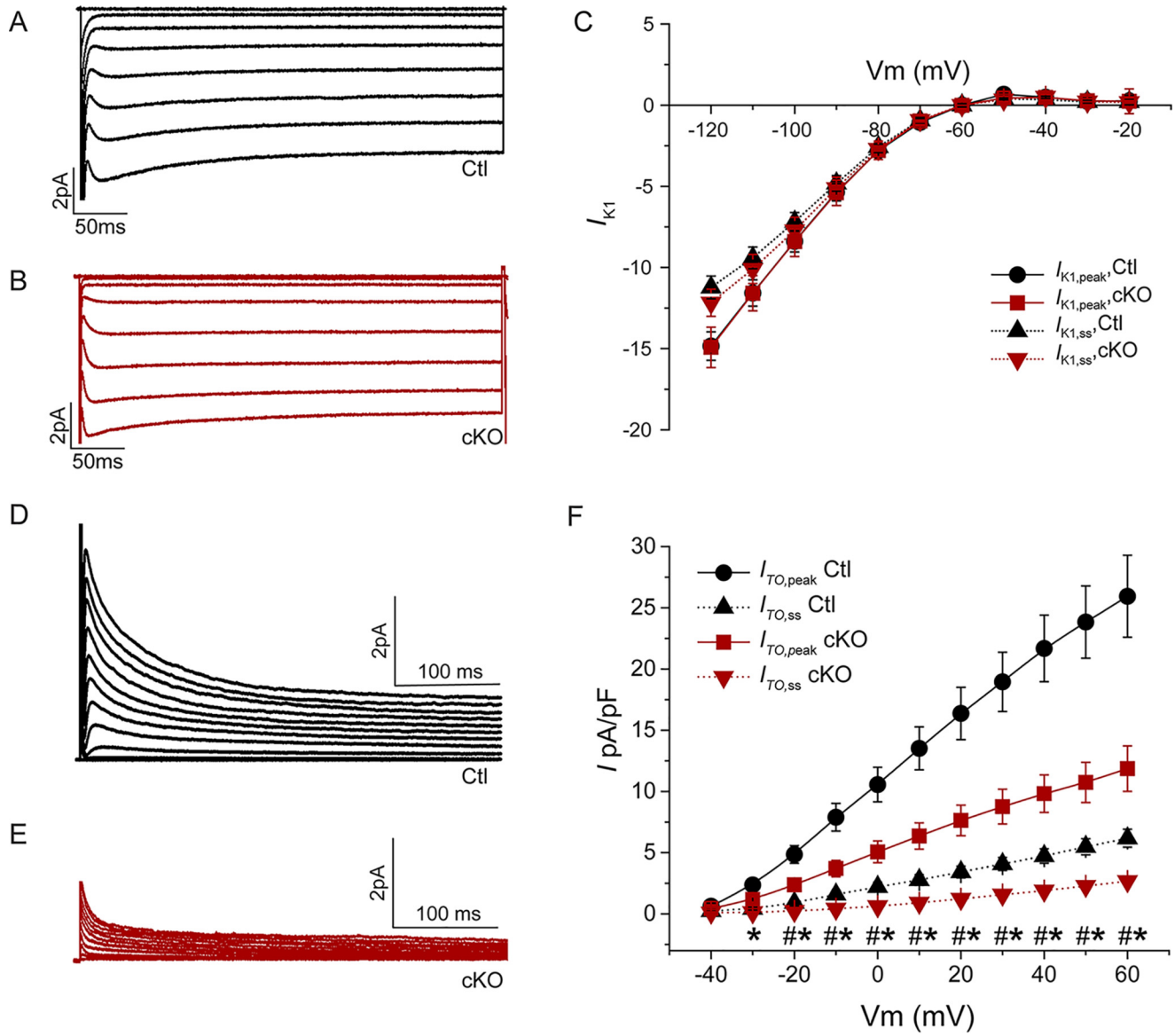


**Figure 8. αII spectrin cKO myocytes display altered $I_{TO}$.** *A–C,* representative recordings of whole cell $I_{K1}$ from cardiomyocytes isolated from control (*A*) and αII spectrin (*B*) cKO mice at 12–16 weeks of age. *C,* current-voltage relationship, of $I_{K1,peak}$ and $I_{K1,SS}$ in αII spectrin cKO and control ventricular myocytes ($n = 4$ and 2; $n = 16$ and 6 for control and αII spectrin cKO, respectively). *D–F,* representative recordings of whole cell $I_{TO}$ from control (*D*) and αII spectrin (*E*) cKO cardiomyocytes. *F,* current-voltage relationship of $I_{TO,peak}$ and $I_{TO,SS}$ in αII spectrin cKO and control ventricular myocytes from 12- to 16–week-old mice ($n = 3$ and 3; $n = 10$ and 13 for control and αII spectrin cKO, respectively). Values are represented as mean ± S.E. * and # indicate a statistically significant difference between genotypes at a given voltage in $I_{TO,peak}$ and $I_{TO,SS}$, respectively.

phy (decreased left ventricular posterior wall (LVPW) thickness (Fig. 10*C*)) compared with control TAC littermates. Furthermore, compared with control TAC littermates, αII spectrin cKO TAC mice displayed more pronounced ECG changes, including QT and QTc prolongation, and T-wave depression (Fig. 10, *F* and *G*, Table S2). Additionally, histologic analysis with automated quantification of fibrosis in hearts of αII spectrin cKO and control mice indicated increased fibrosis in αII spectrin cKO hearts following TAC (Fig. S14, *A–C*). TUNEL staining reveled a large, but statistically insignificant ($p = 0.0689$) increase in apoptosis in αII spectrin cKO mice (Figs. S14, *G-I*, and S15), suggesting that the observed fibrosis may be replacement fibrosis. Finally, increased vacuolization of cardiac tissue was observed in αII spectrin cKO mice but not control mice (Fig. S14, *B, C, E,* and *F*). Notably, these changes occur in the absence of generalized disruption of the cardiomyocyte sarcomere or intercalated disc structure (Fig. S16). In summary, αII spectrin is required for normal physiologic cardiac remodeling, as loss of αII spectrin results in accelerated heart failure phenotypes in response to standard experimental models of heart failure and hypertrophy.

## Discussion

Spectrins are broadly expressed, forming a submembrane network with actin essential for membrane organization, flexibility, and stability (8–10). Furthermore, recent work has demonstrated roles for spectrins in the trafficking, regulation, and stabilization of membrane-associated receptors and channels in diverse tissue types (12, 13, 20). Here, we define new roles of αII spectrin in normal cardiac function, *in vivo*. Based on obser-

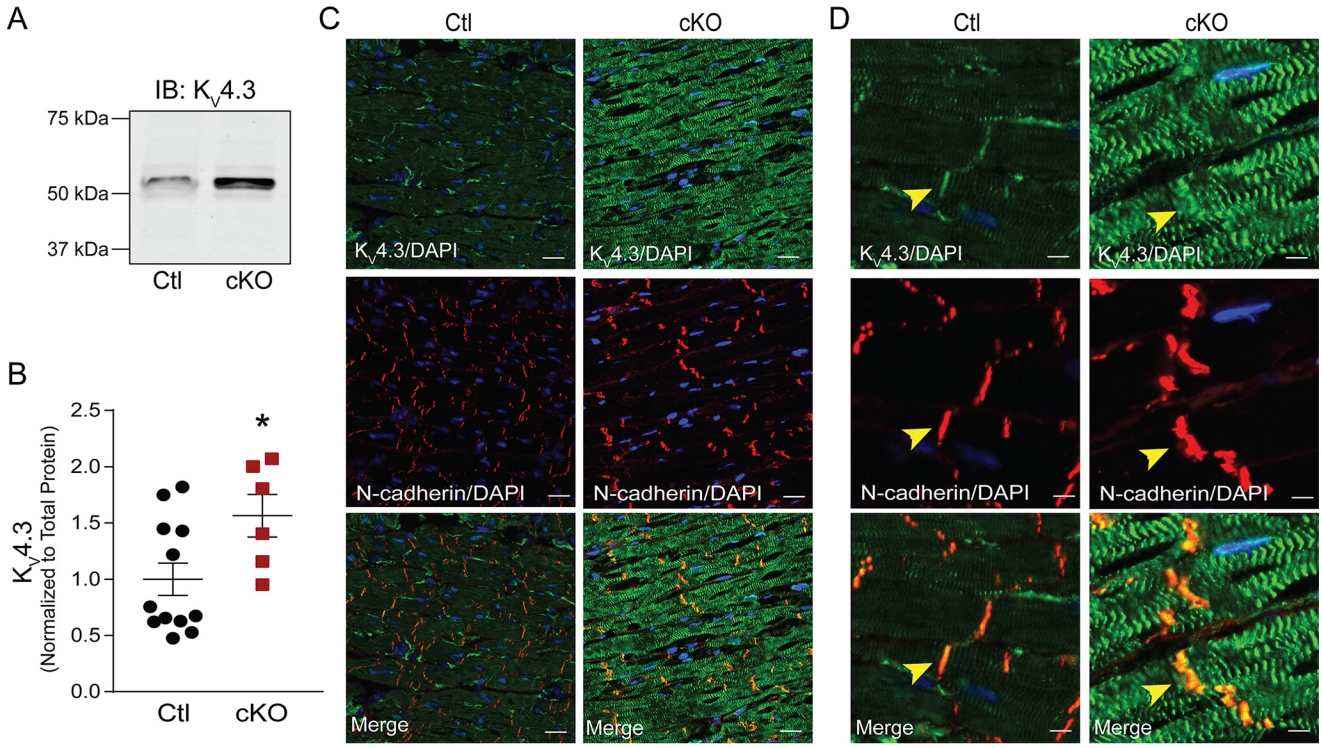


**Figure 9. αII spectrin cKO myocytes display altered K channel expression and localization.** *A,* representative, and *B,* quantification of immunoblots of adult mouse ventricle for $K_V$4.3 ($n = 12$ and 6 for control and αII spectrin cKO, respectively, $p$ value = 0.034 for $K_V$4.3). Values are represented as mean ± S.E. * indicates a statistical differences from controls. *C,* immunofluorescence staining of $K_V$4.3 and N-cadherin in ventricular tissue from control and αII spectrin cKO mice. *Scale bar* = 20 μm. *D,* magnified images of intercalated discs demonstrating reduced intercalated disc localization (*yellow arrowheads*) in αII spectrin cKO tissue. *Scale bar* = 5 μm.

vations of striking alterations in αII spectrin regulation in human heart failure and the lack of knowledge about the role of cardiac αII spectrin, we tested the impact of αII spectrin deficiency on the vertebrate heart. We establish that αII spectrin is required for normal cardiac structure and function, as adult αII spectrin cKO mice display reduced contractility. Histologically, αII spectrin cKO mice display simultaneous increases in cellular hypertrophy and fibrosis. Furthermore, unlike control mice, αII spectrin cKO mice displayed striking mortality in response to standard TAC protocols and significant remodeling and tissue damage in response to a less severe pressure-overload protocol. Underlying this dysfunction, αII spectrin cKO mice demonstrate a trend toward an increase in apoptosis and increased fibrosis following TAC. In addition to structural phenotypes, αII spectrin cKO mice display electrical phenotypes at baseline that are exacerbated in response to catecholamines. At the molecular level, we illustrate a central role of αII spectrin for the dynamic regulation of global α and β spectrin expression and localization *in vivo*. Furthermore, we illustrate a critical role of αII spectrin in the expression and targeting of $Na_V1.5$ and $K_V4.3$, resulting in reductions of $I_{Na}$ and $I_{TO}$ in the heart. Finally, we define the impact of αII spectrin expression on upstream spectrin regulatory pathways. These findings provide new insight of the central nodal role of αII spectrin in the formation and regulation of key structural, electrical, and signaling pathways in heart.

### *αII spectrin regulates global cardiac spectrin pathways*

αII spectrin is abundantly expressed in the heart where it forms heterotetramers with βI, βII, and βIV spectrin. Importantly, the role of cardiac αII spectrin, specifically, is relatively unexplored. Given the essential role of αII spectrin in excitable cells (21–26, 30, 42), *in vivo* roles of αII spectrin were anticipated. However, the severity of *in vivo* and *in vitro* αII spectrin cKO phenotypes were unexpected, particularly the impact of αII spectrin loss on both α and β spectrin expression. For most functions, the spectrin heterotetramer is the functional unit, with the presence of both α and β spectrin being required for spectrin stability (29). Thus, work on the *in vivo* role of β spectrins provides insight into the function of α spectrins. Cardiomyocyte-specific βII spectrin-deficient (βII spectrin cKO) mice experience a variety of electrophysiological abnormalities, including increased heart rate variability, atrioventricular block, prolonged QT intervals, and widened QRS complexes at baseline, along with pronounced ventricular arrhythmias and death following catecholaminergic stress (19). Similar to αII spectrin cKO mice, βII spectrin cKO mice displayed accelerated heart failure phenotypes following transverse aortic constriction. The near absence of βII spectrin in the αII spectrin model (that did not display such striking electrical phenotypes) supports that remodeling of other cardiac pathways is sufficient to mitigate more severe phenotypes.

### *αII spectrin relationship with αI spectrin*

Cardiac αII spectrin localizes to the Z-disc, lateral membrane, and intercalated disc. Alternately, αI spectrin is localized only to the Z-disc and lateral membrane, leaving αII spectrin as the only α spectrin at the intercalated disc. Although we hypothesized that this would lead to deficits in intercalated disc organization and function in αII spectrin cKO mice, we were

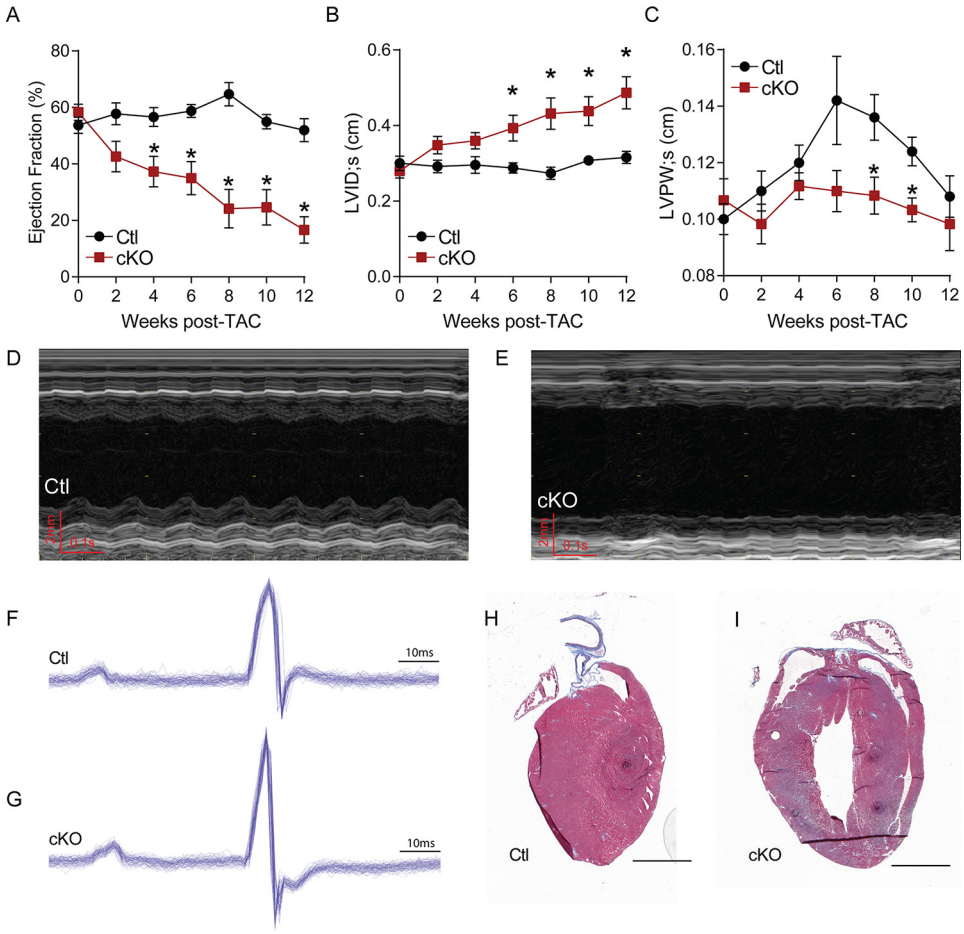


**Figure 10. αII spectrin cKO mice exhibit accelerated heart failure phenotypes following TAC.** *A–D*, following TAC, αII spectrin cKO mice have decreased cardiac function, as evaluated by echocardiography. *A*, ejection fraction decreased precipitously in αII spectrin cKO mice, whereas, *B*, LVID at systole, increases compared with control mice. *C*, LVPW at systole failed to increase in αII spectrin cKO mice. *D* and *E*, representative M-mode traces from control (*D*) and αII spectrin (*E*) cKO mice at 12 weeks following TAC ($n = 5$ and 6 for control and αII spectrin cKO mice, respectively). *F* and *G*, representative ECG traces from control (*F*) and αII spectrin (*G*) cKO mice demonstrating T-wave depression ($n = 5$ and 6 for control and αII spectrin cKO mice, respectively). *H* and *I*, representative images of cardiac structure in control (*H*) and αII spectrin (*I*) cKO mice. *Scale bar* indicates 2 mm ($n = 3$ and 4 for control and αII spectrin cKO mice, respectively). All values are represented as mean ± S.E. * indicates a statistical differences from controls, $p < 0.05$.

surprised to observe translocation of αI spectrin to the intercalated disc in the absence of cardiac αII spectrin (Fig. 5). This change in localization, along with a somewhat mild phenotype at baseline suggests functional redundancy among cardiac α spectrins, and a partial compensation by αI spectrin for αII spectrin loss. This is, perhaps not surprising, as only mammals have two α spectrin genes, αI having arisen from a gene duplication in terrestrial vertebrates (43). However, it is apparent from our characterization of αII spectrin cKO mice that this compensation is not complete. Although young, unchallenged mice are able to maintain normal cardiac function and conduction, age, physiologic (catecholamines) and pathologic (TAC) stress resulted in dysfunction. Although compensatory dysregulation of the spectrin cytoskeleton and opposing reductions of currents in the heart are able to preserve cardiac function at baseline, even somewhat subtle disruptions (age, mild pressure overload) resulted in a failure to maintain cardiac function, resulting in reduced contractility and arrhythmia. This is likely due to the relative inability of αI spectrin to associate with αII spectrin targets.

When cardiac βII spectrin is knocked out, there is an up-regulation of other β spectrins, whereas α spectrins are decreased. The opposite is observed here, with loss of αII spectrin causing an increase in αI spectrin and a decrease in β spectrins. Based on these observations and on the nature of α-β spectrin tetramer formation, we hypothesize the dysregulation occurs due to increased degradation of unbound spectrin monomers, which are unable to form stable α-β tetramers due to perturbed ratios of α and β spectrins.

### αII spectrin regulates cardiac $I_{TO}$

The relatively normal action potential duration in αII spectrin cKO mice supports the impressive pathways likely evolved in cardiac tissue to maintain excitability. The association of αII spectrin with $Na_V1.5$ was not unexpected (3, 5). However, our new findings illustrate altered $K_V4.3$ and $I_{TO}$ in αII spectrin cKO myocytes. Although co-immunoprecipitation experiments demonstrate association of αII spectrin with $K_V4.3$ (and $Na_V1.5$), the relationship of these proteins may be indirect and instead related to secondary cytoskeletal interactions or functional interactions between channel subunits. Prior work from Remme and colleagues (44) has elegantly demonstrated regulation of $I_{Na}$ by $K_V4.3$, beyond electrophysiologic interference. Furthermore, work by Deschênes *et al.* (45) has demonstrated

physical association of subunits responsible for $I_{Na}$ and $I_{TO}$ in neonatal rat ventricular myocytes. Given the dependence of both currents on αII spectrin for stability at the membrane, it is also possible that there is a co-trafficking mechanism contributing to their concurrent reductions, as has been observed between $Na_V1.5$ and $K_{ir}2.1$ (46). Whether $I_{TO}$ ($K_V4.3$) remodeling is a direct impact of αII spectrin loss, or a secondary compensatory factor to preserve action potential dynamics will be an important future area for research (43).

Although our study notes extensive transcriptional dysregulation in hearts lacking αII spectrin, similar to the dysregulation observed following the loss of binding partner, ankyrin G (5), the mechanism of this dysregulation is not known. Although αII spectrin does localize (albeit at low levels) to the nucleus and is known to play a role in DNA repair (47, 48), a role for αII spectrin in direct transcriptional regulation in heart has not been described to our knowledge. It is likely that the transcriptional changes observed are a cellular response to the described disruptions of the cytoskeleton network, however, the mechanism of this regulation remains unexplored.

There are important aspects of the αII spectrin cKO mouse phenotype that are not yet fully elucidated. First, the normal dV/dt in the setting of reduced $I_{Na}$ is surprising, and is incompletely explained by the simultaneous reduction in $I_{TO}$. Furthermore, fibrosis and hypertrophy were observed to occur simultaneously, preventing an investigation of any potential causal relationship. These limitations elucidate important areas for future study.

It is important to note that although experiments were done using isolated cardiomyocytes when possible (electrophysiology, immunoblotting), experiments conducted on whole heart tissue (RNAseq, histology) are confounded by the presence of noncardiomyocytes in heart tissue. Although efforts were made to obtain the most cardiomyocyte-rich sample possible, the contribution of blood, fibroblasts, adipocytes, and immune cells cannot be eliminated.

Finally, heart failure results in dysregulated calcium handling, which can contribute to increased calcium-activated calpain activity. We have shown increased calpain-mediated degradation of αII spectrin is associated with heart failure. Consistent with our new findings, work from Jain *et al.* (24) have previously demonstrated αII spectrin breakdown products in the serum of neonates with congenital heart disease. However, future studies investigating the localization of αII spectrin and other spectrins in human heart failure, in addition to the potential effect of αII and βII spectrin degradation in heart failure are essential to further our understanding of the role of spectrin dysregulation in both congenital and acquired heart failure.

## Experimental procedures

### Human heart tissue

Ischemic and nonischemic failing left ventricular tissue samples from explanted hearts of patients undergoing heart transplantation were obtained through The Cooperative Human Tissue Network: Midwestern Division at The Ohio State University. Nonfailing hearts were obtained through the Lifeline of Ohio Project. The Ohio State University Institutional Review Board approved the use of human subject tissue. This investigation conforms to the principles outlined in the Declaration of Helsinki.

### Animal studies

Cardiomyocyte-specific αII spectrin knockout (αII spectrin cKO) mice were produced using the Cre-flox system. Mice with exon 8 of the *Sptan1* gene flanked by LoxP sites ($Sptan1^{f/f}$ mice) (30) were backcrossed onto a C57BL/6J background for greater than five generations. Mice with Cre recombinase expression driven by the α-myosin heavy chain promoter were acquired from Jackson Laboratories (B6N.FVB(B6)-Tg(Myh6-cre)2182Mds/J, stock number 018972). $Sptan1^{f/WT}$ breeders were established by maintaining one cre-positive parent per breeding pair. The genotype was confirmed with PCR (primers: Cre forward, ATGACAGACAGATCCCTCCTATCTCC; Cre reverse, CTCATCACTCGTTGCATCATCGAC; Cre internal control forward, CAAATGTTGCTTGTCTGGTG; Cre internal control reverse, GTCAGTCGAGTGCACAGTTT; *Sptan1*flox forward, AACAGTCACACCCTCTGAGTGCCA; *Sptan1*flox reverse, ATTCAGTGGAAAGCTGAGAAGCCAG). Male and female mice between 16 and 24 weeks of age were used for experiments, unless otherwise noted. Littermate $Sptan1^{WT/WT}$, $Cre^+$, or $Sptan1^{f/f}$ $Cre^-$ mice were used as controls for $Sptan1^{f/f}$, $Cre^+$, and αII spectrin cKO mice. Young mice were between 12 and 16 weeks of age. Adult mice were 20–24 weeks of age. The Ohio State University IACUC approved all animal studies. The investigation conformed to the Guide for the Care and Use of Laboratory Animals published by the NIH.

### Echocardiography

Echocardiographic analysis was performed on mice lightly anesthetized with isoflurane (1.75% in 1 liter/min oxygen). Mice were immobilized on a heated imaging stage during image acquisition. HR was monitored throughout imaging and recordings that obtained heart rates ≤400 bpm were excluded. Long and short axis analyses were conducted using the GE LOGIQ E, whereas Doppler analysis was conducted on a VEVO 2100. Analysis was conducted following acquisition using at least three nonadjacent contractions. Researchers blinded to genotype performed the image collection and analysis.

### Electrocardiogram

Surface electrocardiogram analysis was conducted on mice anesthetized with isoflurane (2% in 1 liter/min oxygen). Mice were immobilized on a heated imaging stage during acquisition. Lead II ECGs were collected using PowerLab equipment (ADInstruments). Conscious ECGs were collected using: 1) the ECGenie system with eMouse analysis software (Mouse-Specific Inc.) or 2) implanted radiotelemetry using an ETA-F10 miniature telemeter (DSI) and Ponemah acquisition software. All conscious ECGs were analyzed using LabChart software. Researchers blinded to genotype performed the collection and analysis.

### Transverse aortic constriction

Mice were anesthetized with 2% isoflurane and intubated for artificial ventilation at 120–160 breaths per minute, tidal vol-

ume of 0.2–0.35 ml. Heating pads were used to keep body temperatures at 37 °C throughout the procedure. The transverse aorta was accessed via a left lateral thoracotomy and 6-0 suture is used to ligate the aorta overlying a blunted 25- or 27-gauge needle. The needle was removed immediately following ligation leaving a discrete region of stenosis of the aorta. Successful constriction was confirmed by measuring the velocity of blood flow at the aortic root and after the construction site using echocardiography. The surgeon was blinded to genotype.

### Cardiomyocyte isolation

Adult cardiomyocytes were isolated using aortic cannulation and retroperfusion of enzymes (for action potential and sodium current recordings, protease and collagenase type II (Worthington biochemical) or for potassium current recordings, Liberase TH (Roche Applied Science)) into the coronary circulation, as previously described (49–51). Following isolation, cells were fixed with ethanol for staining, lysed for immunoblot, or processed for electrophysiology experiments.

### Cardiac histologic analysis

Hearts were excised and flash frozen or fixed in 4% paraformaldehyde for 24 h. Masson's trichrome staining was performed on 5-μm sections at the Comparative Pathology and Mouse Phenotyping Lab at the Ohio State University. TUNEL staining was performed using a fluorescein *in situ* cell death detection kit (Roche, 11684795910). Whole heart images were collected using a PathScan Enabler IV. Images of cross-sectional myocytes from Masson's trichrome-stained and TUNEL-stained cardiac sections were collected on an EVOS microscope (Thermo Scientific). Cross-sectional areas of 50 myocytes per sample were measured using ImageJ software (52). Researchers blinded to genotype performed the image collection and analysis. Levels of fibrosis were quantified using an add-on to MATLAB (Mathworks). The add-on converts images from the RGB color space into CIELAB color space, then segments the images using the $k_{means}$ algorithm. Finally, the fibrosis (blue) segment is filtered through a color mask to remove noise, and the ratio of fibrosis to other tissues was calculated. TUNEL-stained images were analyzed using ImageJ "Color Threshold" and "Analyze Particles" functions. Only particles between 200 and 5000 pixels were counted as nuclei. Numbers of TUNEL-positive nuclei were normalized to total nuclei (by 4′,6-diamidino-2-phenylindole).

### Immunoblotting

Cardiomyocytes or ventricular tissue samples were homogenized using a Cryolys-cooled Precellys 24-bead homogenizer (Bertin Corp.) using a combination of 1.4- and 2.8-mm ceramic beads at 6000 rpm for three bouts of 15 s in homogenization buffer (0.025 M Tris-HCl, 0.15 M NaCl, 0.001 M EDTA, 1% (v/v) Nonidet P-40, 5% (v/v) glycerol, pH 7.4). Homogenates were then centrifuged for 30 min at 21,130 × *g* at 4 °C. Following quantification by a BCA assay (Pierce), lysates were separated on 4–15% precast ProteanTGX gels (Bio-Rad) and transferred to nitrocellulose membranes. Membranes were incubated in primary antibody overnight at 4 °C. Primary antibodies targeted αI spectrin (BioLegend; 803101), αII spectrin (BioLegend; 803201), β1 spectrin (ThermoFisher; MA3-062), βII spectrin (Custom from Covance), Kv4.3 (Neuromab; clone K75/41), $Na_V1.5$ (Covance (3)), Mena (a generous gift from Dr. Benz), and Vasp (ImmunoGlobe; 0012-02). Secondary antibodies used were donkey anti-rabbit or donkey anti-mouse (Jackson ImmunoResearch Laboratories, Bio-Rad). Densitometric analysis was performed using ImageJ.

### Immunofluorescence

Isolated cardiomyocytes or cryopreserved cardiac tissue cryosliced at 5 μm were blocked with fish gelatin buffer (3% fish gelatin, 0.1% DMSO, 0.075% Triton X-100) and incubated with primary antibody in fish gelatin buffer overnight at 4 °C. Primary antibodies targeted αI spectrin (BioLegend; 803101), αII spectrin (BioLegend; 803201), β1 spectrin (ThermoFisher; MA3-062), βII spectrin (Covance), Kv4.3 (Neuromab; clone K75/41), $Na_V1.5$ (Covance (3)), Mena (a generous gift from Dr. Benz), Vasp (ImmunoGlobe; 0012-02), NCAD (ThermoFisher, 33-3900), Desmin (Sigma), or α-actinin (Sigma). Following incubation with secondary antibodies (donkey anti-rabbit 568 and donkey anti-mouse 488) in fish gelatin buffer for 4 h at room temperature, samples were washed repeatedly with fish gelatin buffer, mounted with Vectashield (Vector Laboratories), covered with a coverslip, and sealed. Secondary antibody staining controls were conducted for each tissue preparation. Images were acquired at room temperature using an LSM 780 AxioObserver microscope (Zeiss) (40 × 1.30 NA lens, pinhole = 1.0 airy disc) and analyzed using ZEN imaging software (Zeiss). Samples from at least three mice were used for each experiment, and at least three representative images per animal per stain were acquired. Images were collected by a blinded researcher using identical detector gain and acquisition settings for all samples within an experiment.

### Single-cell electrophysiology

Sodium current ($I_{Na}$) recordings were conducted in a low-sodium extracellular solution containing (in mM): NaCl, 10; $MgCl_2$, 1; $CaCl_2$, 1.8; $CdCl_2$, 0.1; HEPES, 20; CsCl, 127.5; glucose, 11. The pipette solution contained (in mM): NaCl, 5; CsF, 135; EGTA, 10; MgATP, 5; HEPES, 5. To characterize the voltage dependence of the peak $I_{Na}$, single cells were held at −120 mV, and 200 ms voltage steps were applied from −100 to +10 mV in 5 mV increments. The interval between voltage steps was 3 s. Action potentials were elicited using square wave pulses (1–2 nA amplitude, 2–3 ms duration) generated by a DS8000 digital stimulator (World Precision Instruments, Sarasota, FL) and recorded at room temperature with a pipette solution containing (in mM): $MgCl_2$ (1), EGTA (1), KCl (150), HEPES (5), phosphocreatine (5), $K_2ATP$ (4.46), β-hydroxybutyric acid (2), adjusted to pH 7.2 with KOH; and extracellular solution containing (in mM): NaCl (148), $NaH_2PO_4$ (0.4), $MgCl_2$ (1), glucose (5.5), KCl (5.4), $CaCl_2$ (1), HEPES (15), EGTA (1), adjusted to pH 7.2 with NaOH. The transient outward $K^+$ current ($I_{TO}$) recordings were conducted at room temperature. The bath solution contained (in mM): NaCl (136), KCl (4), $CaCl_2$ (1.8), $MgCl_2$ (2), HEPES (10), tetrodotoxin (0.03), nifedipine (0.005), pH adjusted at 7.4 with NaOH. Recording pipettes contained (mM): KCl (135), $MgCl_2$ (1), EGTA (10), HEPES (10), glucose

(5), adjusted to pH 7.2 with KOH. $I_{TO}$ was recorded using a step protocol with a holding potential of −70 mV and stepping from −40 to + 60 mV in 10-mV increments of 5 s at each potential, every 20 s. Peak $I_{TO}$ was measured as the steady-state current at the end of the 5-s pulse.

### RNA sequencing

RNA-Seq of RNA isolated from male and female αII spectrin cKO and littermate control mice was conducted in collaboration with Ocean Ridge BioSciences (Deerfield Beach, FL). Mice were sacrificed using an isoflurane overdose, and the heart were immediately excised. The aorta was then cannulated and the heart was retroperfused with ice-cold Hanks' balanced salt solution to remove blood contamination. Ventricles were snap-frozen in liquid nitrogen. Total RNA was isolated from the tissue using the TRI Reagent® (Molecular Research Center, part number TR118). Total RNA was quantified and assessed for quality on a 1% agarose, 2% formaldehyde gel. The RNA was then treated with RNase-free DNase I (Epicenter; part number D9905K) and re-purified using Agencourt RNAClean XP beads (Beckman Coulter; part number A63987). Final RNA samples were then quantified by spectrophotometry. cDNA libraries were prepared from 250 ng of DNA-free total RNA using the TruSeq Stranded mRNA Library Prep (96 samples) (Illumina Inc.; part number 20020595). The quality and size distribution of the amplified libraries were determined by CHIP-based capillary electrophoresis (Bioanalyzer 2100, Agilent Technologies). Libraries were Bioanalyzed (Bioanalyzer 2100, Agilent Technologies) and quantified using the KAPA Library Quantification Kit (Kapa Biosystems, Boston, MA). The libraries were loaded onto an Illumina HiSeq 4000 flowcell and bridge amplified to create sequence clusters and sequenced with 150 nucleotide paired-end reads plus dual index reads.

Quality-filtered and base-trimmed reads were used for alignment. Sequence alignment was performed using HISAT2 version 2.0.5. The read summarization program feature Counts2 version 1.5.1 was used for exon- and gene-level counting. Normalized RPKM values were calculated from the raw feature Counts read, and were then filtered to retain a list of genes with a minimum of ~50 mapped reads in 25% or more samples. The threshold of 50 mapped reads is considered the Reliable Quantification Threshold. GO Pathway Analysis was conducted to guide analysis and interpretation.

### Co-immunoprecipitation

Co-immunoprecipitation experiments were conducted as previously described(53). WT mouse heart samples were homogenized in buffer (containing 0.025 M Tris-HCl, 0.15 M NaCl, 0.001 M EDTA, 1% (v/v) Nonidet P-40, 5% (v/v) glycerol, pH 7.4) using a Dounce homogenizer. Lysates were centrifuged for 30 min at 13,000 rpm at 4 °C on using a benchtop centrifuge. One mg of supernatant was incubated and rotated with 2 μg of Kv4.3 (Neuromab; clone K75/41), $Na_V1.5$ (Covance (3)), Mena (a generous gift from Dr. Benz), or control IgG at 4 °C overnight. Following incubation, lysates with antibodies were rotated with washed Protein A/G Magnetic Beads (Pierce, number 88802) for 5 h at 4 °C. After a 5-h incubation, the supernatant was removed from the beads using a magnetic stand, and the beads were washed 3 times with PBS. Bound protein was eluted with 2× Laemmli sample buffer and β-mercaptoethanol and heated to 95 °C for 10 min before immunoblotting with αI spectrin (BioLegend; 803101) or αII spectrin (BioLegend; 803201) antibodies. 60 μg of lysate was used as an input loading control for each experiment.

### Statistical analysis

All continuous variables are represented as mean ± S.E. A multivariate one-way analysis of variance with Tukey's Honestly Significant Difference post hoc was used to identify differences among groups when data were normally distributed (passed Shapiro-Wilk normality test) in experiments with greater than two experimental groups. For experiments with just two experimental groups, an unpaired two-tailed Student's *t* test was performed, provided data were normally distributed based on a Shapiro-Wilk normality test. When data failed to pass a normality test, a Mann-Whitney test was performed. For experiments where the same mice were followed over time (TAC mice), a repeated measured two-way (genotype by time) analysis of variance was conducted. When examining differences in a categorical variable (failure to capture) between genotypes, a Fisher's exact test was used. Differences were considered significant at $p < 0.05$. Statistical analysis was performed using SPSS 25.0 (IBM SPSS Statistics) and GraphPad Prism (version 7.01 for Windows, GraphPad Software).

*Author contributions*—E. R. L., M. N. R., T. J. H., and P. J. M. conceptualization; E. R. L., N. P. M., H. M., M. V. P., J. L. W., and T. J. H. data curation; E. R. L., N. P. M., M. V. P., M. H., M. E. R., X. X., N. K. H., S. N. K., and T. J. H. formal analysis; E. R. L., N. P. M., H. M., and C. Y.-M. H. validation; E. R. L., N. P. M., H. M., R. G., M. V. P., M. H., G. E. D., D. G., M. E. R., X. X., N. K. H., E. L. F., P. L., M. J. W., O. C., S. L. S., J. L. W., M. S., S. N. K., and P. M. J. investigation; E. R. L., N. P. M., and H. M. visualization; E. R. L., N. P. M., H. M., G. E. D., X. X., O. C., S. N. K., P. M. J., and T. J. H. methodology; E. R. L. and T. J. H. writing-original draft; E. R. L., S. N. K., P. M. J., M. N. R., and T. J. H. project administration; E. R. L., N. P. M., H. M., C. Y.-M. H., M. E. R., S. N. K., T. J. H., and P. J. M. writing-review and editing; C. Y.-M. H., P. M. J., and M. N. R. resources; D. G., P. M. J., T. J. H., and P. J. M. funding acquisition.

### References


1. Centers for Disease Control and Prevention and Statistics, N. C. (2015) *f. H. Health, United States, 2014*, Centers for Disease Control and Prevention, Hyattsville, MD
2. Perkins, E., Suminaite, D., and Jackson, M. (2016) Cerebellar ataxias: β-III spectrin's interactions suggest common pathogenic pathways. *J. Physiol.* **594,** 4661–4676 CrossRef Medline
3. Makara, M. A., Curran, J., Little, S. C., Musa, H., Polina, I., Smith, S. A., Wright, P. J., Unudurthi, S. D., Snyder, J., Bennett, V., Hund, T. J., and Mohler, P. J. (2014) Ankyrin-G coordinates intercalated disc signaling platform to regulate cardiac excitability *in vivo*. *Circ. Res.* **115,** 929–938 CrossRef Medline
4. Curran, J., and Mohler, P. J. (2015) Alternative paradigms for ion channelopathies: disorders of ion channel membrane trafficking and posttranslational modification. *Annu. Rev. Physiol.* **77,** 505–524 CrossRef Medline
5. Makara, M. A., Curran, J., Lubbers, E. R., Murphy, N. P., Little, S. C., Musa, H., Smith, S. A., Unudurthi, S. D., Rajaram, M. V. S., Janssen, P. M. L., Boyden, P. A., Bradley, E. A., Hund, T. J., and Mohler, P. J. (2018) Novel

mechanistic roles for ankyrin-G in cardiac remodeling and heart failure. *JACC Basic Transl. Sci.* **3,** 675–689 CrossRef Medline
6. Voas, M. G., Lyons, D. A., Naylor, S. G., Arana, N., Rasband, M. N., and Talbot, W. S. (2007) αII-spectrin is essential for assembly of the nodes of ranvier in myelinated axons. *Curr. Biol.* **17,** 562–568 CrossRef Medline
7. Wang, Y., Ji, T., Nelson, A. D., Glanowska, K., Murphy, G. G., Jenkins, P. M., and Parent, J. M. (2018) Critical roles of αII spectrin in brain development and epileptic encephalopathy. *J. Clin. Invest.* **128,** 760–773 CrossRef Medline
8. Clarke, M. (1971) Isolation and characterization of a water-soluble protein from bovine erythrocyte membranes. *Biochem. Biophys. Res. Commun.* **45,** 1063–1070 CrossRef Medline
9. Marchesi, V. T., and Steers, E., Jr. (1968) Selective solubilization of a protein component of the red cell membrane. *Science* **159,** 203–204 CrossRef Medline
10. Elgsaeter, A., Stokke, B. T., Mikkelsen, A., and Branton, D. (1986) The molecular basis of erythrocyte shape. *Science* **234,** 1217–1223 CrossRef Medline
11. Tohyama, J., Nakashima, M., Nabatame, S., Gaik-Siew, C., Miyata, R., Rener-Primec, Z., Kato, M., Matsumoto, N., and Saitsu, H. (2015) SPTAN1 encephalopathy: distinct phenotypes and genotypes. *J. Hum. Genet.* **60,** 167–173 CrossRef Medline
12. Bennett, V., and Healy, J. (2008) Organizing the fluid membrane bilayer: diseases linked to spectrin and ankyrin. *Trends Mol. Med.* **14,** 28–36 CrossRef Medline
13. Machnicka, B., Czogalla, A., Hryniewicz-Jankowska, A., Bogusławska, D. M., Grochowalska, R., Heger, E., and Sikorski, A. F. (2014) Spectrins: a structural platform for stabilization and activation of membrane channels, receptors and transporters. *Biochim. Biophys. Acta* **1838,** 620–634 CrossRef Medline
14. Bennett, V., and Baines, A. J. (2001) Spectrin and ankyrin-based pathways: metazoan inventions for integrating cells into tissues. *Physiol. Rev.* **81,** 1353–1392 CrossRef Medline
15. Zhang, R., Zhang, C., Zhao, Q., and Li, D. (2013) Spectrin: structure, function and disease. *Sci. China Life Sci.* **56,** 1076–1085 CrossRef Medline
16. Djinovic-Carugo, K., Gautel, M., Ylänne, J., and Young, P. (2002) The spectrin repeat: a structural platform for cytoskeletal protein assemblies. *FEBS Lett.* **513,** 119–123 CrossRef Medline
17. Hamdan, F. F., Saitsu, H., Nishiyama, K., Gauthier, J., Dobrzeniecka, S., Spiegelman, D., Lacaille, J. C., Décarie, J. C., Matsumoto, N., Rouleau, G. A., and Michaud, J. L. (2012) Identification of a novel in-frame *de novo* mutation in SPTAN1 in intellectual disability and pontocerebellar atrophy. *Eur. J. Hum. Genet.* **20,** 796–800 CrossRef Medline
18. Nonoda, Y., Saito, Y., Nagai, S., Sasaki, M., Iwasaki, T., Matsumoto, N., Ishii, M., and Saitsu, H. (2013) Progressive diffuse brain atrophy in West syndrome with marked hypomyelination due to SPTAN1 gene mutation. *Brain Dev.* **35,** 280–283 CrossRef Medline
19. Derbala, M. H., Guo, A. S., Mohler, P. J., and Smith, S. A. (2018) The role of βII spectrin in cardiac health and disease. *Life Sci.* **192,** 278–285 CrossRef Medline
20. Hund, T. J., Koval, O. M., Li, J., Wright, P. J., Qian, L., Snyder, J. S., Gudmundsson, H., Kline, C. F., Davidson, N. P., Cardona, N., Rasband, M. N., Anderson, M. E., and Mohler, P. J. (2010) A β(IV)-spectrin/CaMKII signaling complex is essential for membrane excitability in mice. *J. Clin. Invest.* **120,** 3508–3519 CrossRef Medline
21. Bennett, P. M., Baines, A. J., Lecomte, M. C., Maggs, A. M., and Pinder, J. C. (2004) Not just a plasma membrane protein: in cardiac muscle cells α-II spectrin also shows a close association with myofibrils. *J. Muscle Res. Cell Motil.* **25,** 119–126 CrossRef Medline
22. Weiss, E. S., Wang, K. K., Allen, J. G., Blue, M. E., Nwakanma, L. U., Liu, M. C., Lange, M. S., Berrong, J., Wilson, M. A., Gott, V. L., Troncoso, J. C., Hayes, R. L., Johnston, M. V., and Baumgartner, W. A. (2009) αII-Spectrin breakdown products serve as novel markers of brain injury severity in a canine model of hypothermic circulatory arrest. *Ann. Thorac. Surg.* **88,** 543–550 CrossRef Medline
23. Zhang, Y., Resneck, W. G., Lee, P. C., Randall, W. R., Bloch, R. J., and Ursitti, J. A. (2010) Characterization and expression of a heart-selective alternatively spliced variant of αII-spectrin, cardi+, during development in the rat. *J. Mol. Cell Cardiol.* **48,** 1050–1059 CrossRef Medline
24. Jain, P., Spaeder, M. C., Donofrio, M. T., Sinha, P., Jonas, R. A., and Levy, R. J. (2014) Detection of αII-spectrin breakdown products in the serum of neonates with congenital heart disease. *Pediatr. Crit. Care Med.* **15,** 229–235 CrossRef Medline
25. Baines, A. J., and Pinder, J. C. (2005) The spectrin-associated cytoskeleton in mammalian heart. *Front. Biosci.* **10,** 3020–3033 CrossRef Medline
26. Ursitti, J. A., Petrich, B. G., Lee, P. C., Resneck, W. G., Ye, X., Yang, J., Randall, W. R., Bloch, R. J., and Wang, Y. (2007) Role of an alternatively spliced form of αII-spectrin in localization of connexin 43 in cardiomyocytes and regulation by stress-activated protein kinase. *J. Mol. Cell Cardiol.* **42,** 572–581 CrossRef Medline
27. Yan, X. X., Jeromin, A., and Jeromin, A. (2012) Spectrin breakdown products (SBDPs) as potential biomarkers for neurodegenerative diseases. *Curr. Transl. Geriatr. Exp. Gerontol. Rep.* **1,** 85–93 CrossRef Medline
28. Hill, R. L., Singh, I. N., Wang, J. A., and Hall, E. D. (2017) Time courses of post-injury mitochondrial oxidative damage and respiratory dysfunction and neuronal cytoskeletal degradation in a rat model of focal traumatic brain injury. *Neurochem. Int.* **111,** 45–56 CrossRef Medline
29. Stankewich, M. C., Cianci, C. D., Stabach, P. R., Ji, L., Nath, A., and Morrow, J. S. (2011) Cell organization, growth, and neural and cardiac development require αII-spectrin. *J. Cell Sci.* **124,** 3956–3966 CrossRef Medline
30. Huang, C. Y., Zhang, C., Ho, T. S., Oses-Prieto, J., Burlingame, A. L., Lalonde, J., Noebels, J. L., Leterrier, C., and Rasband, M. N. (2017) αII-Spectrin forms a periodic cytoskeleton at the axon initial segment and is required for nervous system function. *J. Neurosci.* **37,** 11311–11322 CrossRef Medline
31. Subramaniam, A., Jones, W. K., Gulick, J., Wert, S., Neumann, J., and Robbins, J. (1991) Tissue-specific regulation of the α-myosin heavy chain gene promoter in transgenic mice. *J. Biol. Chem.* **266,** 24613–24620 Medline
32. Baines, A. J. (2009) Evolution of spectrin function in cytoskeletal and membrane networks. *Biochem. Soc. Trans.* **37,** 796–803 CrossRef Medline
33. Komada, M., and Soriano, P. (2002) βIV-Spectrin regulates sodium channel clustering through ankyrin-G at axon initial segments and nodes of ranvier. *J. Cell Biol.* **156,** 337–348 CrossRef Medline
34. Uemoto, Y., Suzuki, S., Terada, N., Ohno, N., Ohno, S., Yamanaka, S., and Komada, M. (2007) Specific role of the truncated βIV-spectrin Sigma6 in sodium channel clustering at axon initial segments and nodes of ranvier. *J. Biol. Chem.* **282,** 6548–6555 CrossRef Medline
35. Chen, Q., Li, Z., and Hua, X. (2018) Fate of estrogens in a pilot-scale step-feed anoxic/oxic wastewater treatment system controlling by nitrogen and phosphorus removal. *Environ. Sci. Pollut. Res. Int.* **25,** 12981–12991 CrossRef Medline
36. Onal, B., Gratz, D., and Hund, T. (2016) LongQt: a cardiac electrophysiology simulation platform. *MethodsX* **3,** 589–599 CrossRef Medline
37. Hund, T. J., Decker, K. F., Kanter, E., Mohler, P. J., Boyden, P. A., Schuessler, R. B., Yamada, K. A., and Rudy, Y. (2008) Role of activated CaMKII in abnormal calcium homeostasis and I(Na) remodeling after myocardial infarction: insights from mathematical modeling. *J. Mol. Cell Cardiol.* **45,** 420–428 CrossRef Medline
38. Onal, B., Gratz, D., and Hund, T. J. (2017) $Ca^{2+}$/calmodulin-dependent kinase II-dependent regulation of atrial myocyte late $Na^{+}$ current, $Ca^{2+}$ cycling, and excitability: a mathematical modeling study. *Am. J. Physiol. Heart Circ. Physiol.* **313,** H1227-H1239 CrossRef Medline
39. Glynn, P., Unudurthi, S. D., and Hund, T. J. (2014) Mathematical modeling of physiological systems: an essential tool for discovery. *Life Sci.* **111,** 1–5 CrossRef Medline
40. Pike, B. R., Flint, J., Dutta, S., Johnson, E., Wang, K. K., and Hayes, R. L. (2001) Accumulation of non-erythroid αII-spectrin and calpain-cleaved αII-spectrin breakdown products in cerebrospinal fluid after traumatic brain injury in rats. *J. Neurochem.* **78,** 1297–1306 CrossRef Medline
41. Smith, S. A., Hughes, L. D., Kline, C. F., Kempton, A. N., Dorn, L. E., Curran, J., Makara, M., Webb, T. R., Wright, P., Voigt, N., Binkley, P. F., Janssen, P. M., Kilic, A., Carnes, C. A., Dobrev, D., *et al.* (2016) Dysfunction of the β2-spectrin-based pathway in human heart failure. *Am. J. Physiol. Heart Circ. Physiol.* **310,** H1583–1591 CrossRef Medline

42. Huang, C. Y., Zhang, C., Zollinger, D. R., Leterrier, C., and Rasband, M. N. (2017) An αII spectrin-based cytoskeleton protects large-diameter myelinated axons from degeneration. *J. Neurosci.* **37,** 11323–11334 CrossRef Medline
43. Salomao, M., An, X., Guo, X., Gratzer, W. B., Mohandas, N., and Baines, A. J. (2006) Mammalian αI-spectrin is a neofunctionalized polypeptide adapted to small highly deformable erythrocytes. *Proc. Natl. Acad. Sci. U.S.A.* **103,** 643–648 CrossRef Medline
44. Portero, V., Wilders, R., Casini, S., Charpentier, F., Verkerk, A. O., and Remme, C. A. (2018) KV4.3 expression modulates NaV1.5 sodium current. *Front. Physiol.* **9,** 178 CrossRef Medline
45. Deschênes, I., Armoundas, A. A., Jones, S. P., and Tomaselli, G. F. (2008) Post-transcriptional gene silencing of KChIP2 and Navβ1 in neonatal rat cardiac myocytes reveals a functional association between Na and Ito currents. *J. Mol. Cell Cardiol.* **45,** 336–346 CrossRef Medline
46. Ponce-Balbuena, D., Guerrero-Serna, G., Valdivia, C. R., Caballero, R., Diez-Guerra, F. J., Jiménez-Vazquez, E. N., Ramírez, R. J., Monteiro da Rocha, A., Herron, T. J., Campbell, K. F., Willis, B. C., Alvarado, F. J., Zarzoso, M., Kaur, K., Pérez-Hernandez, M., *et al.* (2018) Cardiac Kir2.1 and NaV1.5 channels traffic together to the sarcolemma to control excitability. *Circ. Res.* **122,** 1501–1516 CrossRef Medline
47. McMahon, L. W., Zhang, P., Sridharan, D. M., Lefferts, J. A., and Lambert, M. W. (2009) Knockdown of alphaII spectrin in normal human cells by siRNA leads to chromosomal instability and decreased DNA interstrand cross-link repair. *Biochem. Biophys. Res. Commun.* **381,** 288–293 CrossRef Medline
48. Sridharan, D., Brown, M., Lambert, W. C., McMahon, L. W., and Lambert, M. W. (2003) Nonerythroid αII spectrin is required for recruitment of FANCA and XPF to nuclear foci induced by DNA interstrand cross-links. *J. Cell Sci.* **116,** 823–835 CrossRef Medline
49. Li, J., Marionneau, C., Koval, O., Zingman, L., Mohler, P. J., Nerbonne, J. M., and Anderson, M. E. (2007) Calmodulin kinase II inhibition enhances ischemic preconditioning by augmenting ATP-sensitive $K^+$ current. *Channels (Austin)* **1,** 387–394 CrossRef Medline
50. Lou, Q., Belevych, A. E., Radwański, P. B., Liu, B., Kalyanasundaram, A., Knollmann, B. C., Fedorov, V. V., and Györke, S. (2015) Alternating membrane potential/calcium interplay underlies repetitive focal activity in a genetic model of calcium-dependent atrial arrhythmias. *J. Physiol.* **593,** 1443–1458 CrossRef Medline
51. Musa, H., Murphy, N. P., Curran, J., Higgins, J. D., Webb, T. R., Makara, M. A., Wright, P., Lancione, P. J., Lubbers, E. R., Healy, J. A., Smith, S. A., Bennett, V., Hund, T. J., Kline, C. F., and Mohler, P. J. (2016) Common human ANK2 variant confers *in vivo* arrhythmia phenotypes. *Heart Rhythm.* **13,** 1932–1940 CrossRef Medline
52. Schneider, C. A., Rasband, W. S., and Eliceiri, K. W. (2012) NIH Image to ImageJ: 25 years of image analysis. *Nat. Methods* **9,** 671–675 CrossRef Medline
53. El Refaey, M., Musa, H., Murphy, N. P., Lubbers, E. R., Skaf, M., Han, M., Cavus, O., Koenig, S. N., Wallace, M. J., Gratz, D., Bradley, E., Alsina, K. M., Wehrens, X. H. T., Hund, T. J., and Mohler, P. J. (2019) Protein phosphatase 2A regulates cardiac $Na^+$ channels. *Circ. Res.* **124,** 737–746 CrossRef Medline